

# Automated optimization of force field parameters against ensemble-averaged measurements with Bayesian Inference of Conformational Populations

Robert M. Raddi<sup>1</sup> and Vincent A. Voelz<sup>1</sup>

*Department of Chemistry, Temple University, Philadelphia, PA 19122, USA.*

(\*Electronic mail: [vvoelz@temple.edu](mailto:vvoelz@temple.edu))

(Dated: February 20, 2024)

Accurate force fields are essential for reliable molecular simulations. These models are refined against quantum mechanical calculations and experimental measurements, which are subject to random and systematic errors. Bayesian Inference of Conformational Populations (BICePs) is a reweighting algorithm that reconciles simulated ensembles with sparse or noisy observables by sampling the full posterior distribution of conformational populations and experimental uncertainty. In this method, a metric called the BICePs score is used to perform model selection, by calculating the free energy of "turning on" the conformational populations under experimental restraints. This approach, when used with improved likelihood functions to deal with experimental outliers, can be used for force field validation (Raddi et al. 2023). Here, we extend the BICePs approach to perform automated force field refinement while simultaneously sampling the full distribution of uncertainties, using a variational method to minimize the BICePs score. To demonstrate the utility of this method, we refine multiple interaction parameters for a 12-mer HP lattice model using ensemble-averaged distance measurements as restraints. To illustrate the resilience of BICePs in the presence of unknown random and systematic errors, we assess the performance of our algorithm through repeated optimizations and under various extents of experimental error. Our results suggest that variational optimization of the BICePs score is a promising direction for robust and automatic parameterization of molecular potentials.

## I. INTRODUCTION

The accuracy of physical potentials used in molecular simulations continues to improve, especially as training data for fitting energy surfaces from quantum-mechanical calculations becomes more available.<sup>1,2</sup> Of similar importance is developing models that can accurately predict ensemble-averaged experimental measurements. Parameterizing models for this purpose is a nontrivial task that requires continuous refinement of microscopic parameters through iterated sampling of the equilibrium distribution.

Such refinement often involves global minimization of the deviation between experimental measurements (e.g. NMR observables) and theoretical predictions from simulated ensembles (the "forward model"), with several complications to consider. First, the forward model is itself an approximation containing some error. Second, ensemble-averaged experimental measurements can be sparse and/or noisy, susceptible to random and systematic errors, which are often unknown *a priori*. Hence, force field refinement requires a mechanism to integrate these multiple sources of uncertainty to automatically discover the optimal parameter set across multiple systems.

Other challenges arise from practical considerations. The high dimensionality and interdependence of force field parameter space presents a significant challenge for refinement. When parameter spaces are large, reproducibility may also be an issue; ideally, identical experimental data should produce parameterizations that should converge towards the same optimal values. For these reasons, automated optimization procedures with sufficiently smooth and differentiable objective functions are preferred.

Numerous methods<sup>3-6</sup> have been developed to address most of these challenges. However, many algorithms do

not include any treatment of uncertainty in the training data, and others lack gradients for automatic refinement. To address these challenges, Bayesian inference methods have been developed.<sup>3,5,6</sup> These methods estimate a Bayesian posterior distribution of conformational populations by treating molecular simulation predictions as prior information, weighted by a likelihood function constructed from the experimental measurements and their uncertainties. The Bayesian posterior can then be used to optimize the prior.

In this work, we extend the Bayesian Inference of Conformational Populations (BICePs) algorithm<sup>7,8</sup> to perform automated force field refinement. BICePs is a reweighting algorithm that refines structural ensembles against sparse and/or noisy experimental observables, and has been used in many previous applications.<sup>9-12</sup> A key advantage of BICePs is that it does not require uncertainty estimates for the forward model; instead, it infers the posterior distribution of these parameters directly from the data through MCMC sampling. BICePs also computes a free energy-like quantity called the BICePs score that can be used for model selection.<sup>5,8</sup>

More recently, we have equipped BICePs with a replica-averaging forward model, making it a maximum-entropy (MaxEnt) reweighting method, and unique in that no adjustable regularization parameters are required to balance experimental information with the prior.<sup>8</sup> With this new approach, the BICePs score becomes a powerful objective function to select and parameterize optimal models. Here, we show that the BICePs score, which reflects the total evidence for a model, can be used for variational optimization of model parameters. The BICePs score contains a form of inherent regularization, and has specialized likelihood functions that allow for the automatic detection and down-weighting of data points subject to systematic error.<sup>8</sup>

To efficiently optimize complex parameter spaces, we derive the first and second derivatives of the BICePs score. We then show how to perform automatic force field optimization against ensemble-averaged observables for several test systems, including a protein lattice model with adjustable bead interaction strengths, and a von Mises-distributed polymer model.

## II. THEORY

BICePs uses a Bayesian statistical framework to treat the extent of uncertainty in experimental observables,  $\sigma$ , as nuisance parameters. Previous versions of BICePs sampled conformational states  $X$  and uncertainty parameter(s)  $\sigma$  from the Bayesian posterior, which takes the form

$$\underbrace{p(X, \sigma|D)}_{\text{posterior}} \propto \underbrace{p(D|X, \sigma)}_{\text{likelihood}} \underbrace{p(X)p(\sigma)}_{\text{priors}}. \quad (1)$$

Here, the prior  $p(X)$  comes from a theoretical model of conformational state populations (typically from a molecular simulation),  $p(D|X, \sigma)$  is a likelihood function quantifying how well a forward model prediction  $f(X)$  agrees with the experimental data  $D$ , and  $p(\sigma) \sim \sigma^{-1}$  is a non-informative Jeffreys prior.

When BICePs is equipped with a replica-averaged forward model, it becomes a MaxEnt reweighting method in the limit of large numbers of replicas<sup>13–17</sup>. The posterior takes the general form

$$p(\mathbf{X}, \sigma|D) \propto \prod_{r=1}^{N_r} \left\{ p(X_r) \prod_{j=1}^{N_j} \frac{1}{\sqrt{2\pi\sigma_j^2}} \exp \left[ -\frac{(d_j - f_j(\mathbf{X}))^2}{2\sigma_j^2} \right] p(\sigma_j) \right\} \quad (2)$$

where  $\mathbf{X}$  is a set of  $N_r$  conformation replicas,  $d_j$  is an observable in the set of  $N_j$  ensemble-averaged experimental measurements, and  $f_j(\mathbf{X}) = \frac{1}{N_r} \sum_r f_j(X_r)$  is the replica-averaged forward model prediction of observable  $j$ . The  $\sigma_j$  values are nuisance parameters that capture uncertainty in the measurements as well as the replica-averaged forward model. In (2), a Gaussian likelihood is used, but more sophisticated models of uncertainty can be used to capture outliers and systematic error with fewer parameters, as discussed below. Markov chain Monte Carlo (MCMC) is used to sample the posterior.

The replica-averaged forward model  $f(\mathbf{X})$  requires a more sophisticated treatment of uncertainty, since it is approximating the ensemble average as a replica average.<sup>18</sup> Therefore,  $\sigma_j$  becomes a combination of both the Bayesian error  $\sigma_j^B$  and the standard error of the mean sigma  $\sigma_j^{\text{SEM}}$ ,  $\sigma_j = \sqrt{(\sigma_j^B)^2 + (\sigma_j^{\text{SEM}})^2}$ . The finite sampling error,  $\sigma^{\text{SEM}}$  is estimated by taking a windowed average over our finite sample  $f(\mathbf{X})$  as  $\sigma_j^{\text{SEM}} = \sqrt{\frac{1}{N} \sum_r (f_j(X_r) - \langle f_j(\mathbf{X}) \rangle)^2}$ , which decreases as the square root of the number of replicas.

### A. Accounting for systematic error and outliers.

BICePs is equipped with special likelihoods that are very robust in the presence of systematic error. The *Student's* likelihood model is a data error model that marginalizes the uncertainty parameters for individual observables, assuming that the level of noise is mostly uniform, except for a few erratic measurements. This limits the number of uncertainty parameters that need to be sampled, while still capturing outliers.

Consider a model where uncertainties  $\sigma_j$  for particular observables  $j$  are distributed about some typical uncertainty  $\sigma_0$  according to a conditional probability  $p(\sigma_j|\sigma_0)$ . We derive a posterior with a single uncertainty parameter  $\sigma_0$  by marginalizing over all  $\sigma_j$ . For a single replica (for simplicity), the posterior is given by

$$p(X_r, \sigma_0|D) \propto p(X_r) \prod_{j=1}^{N_j} \int_{\sigma^{\text{SEM}}}^{\infty} p(d_j|\mathbf{X}, \sigma_j) p(\sigma_j|\sigma_0) d\sigma_j \quad (3)$$

where  $\sigma_0 = \sqrt{(\sigma^B)^2 + (\sigma^{\text{SEM}})^2}$ .

Modeling the prior on uncertainties  $p(\sigma_j|\sigma_0)$  with a distribution with long tails is very useful because its long tail makes it able to tolerate outliers<sup>18,19</sup>. In most cases, however, it is unclear *a priori* what distribution is best for modeling the input data. To improve the situation, we introduce a model with an additional nuisance parameter  $\beta$ , that is able to tune the extent of the distribution's tail:

$$p(\sigma_j|\sigma_0, \beta) = \frac{\Gamma((\beta+1)/2)}{\Gamma(\beta/2)} \frac{2\beta^\beta \sigma_0^{2\beta-1}}{\sqrt{\beta} \sigma_j^{2\beta}} \exp \left( -\frac{\beta \sigma_0^2}{\sigma_j^2} \right). \quad (4)$$

where  $\sigma_0$  is defined as above, and  $1 \leq \beta < \infty$ . When this distribution is inserted into the posterior, and marginalized over all  $\sigma_j$ , the result is

$$\begin{aligned} p(X_r, \sigma_0, \beta|D) &\propto p(X_r) \prod_{j=1}^{N_j} \int_{\sigma^{\text{SEM}}}^{\infty} \frac{1}{\sqrt{2\pi\sigma_j}} \exp \left( -\frac{(d_j - f_j(\mathbf{X}))^2}{2\sigma_j^2} \right) \\ &\quad \times \frac{\Gamma((\beta+1)/2)}{\Gamma(\beta/2)} \frac{2\beta^\beta \sigma_0^{2\beta-1}}{\sqrt{\beta} \sigma_j^{2\beta}} \exp \left( -\frac{\beta \sigma_0^2}{\sigma_j^2} \right) d\sigma_j \\ &= p(X_r) \prod_{j=1}^{N_j} \frac{\Gamma((\beta+1)/2)}{\Gamma(\beta/2)} \frac{1}{\sqrt{2\pi\beta}\sigma_0} \\ &\quad \times \left[ 1 + \frac{(d_j - f_j(X))^2}{2\beta\sigma_0^2} \right]^{-\beta} \gamma \left( \beta, \frac{(d_j - f_j(X))^2 + 2\beta\sigma_0^2}{2(\sigma^{\text{SEM}})^2} \right), \end{aligned} \quad (5)$$

Here, the marginal likelihood contains the lower incomplete gamma function,  $\gamma$ . We call this the Student's model because it is a variation of Student's *t*-distribution that can be interpolated between functional forms. When  $\beta = 1$ , the model is equivalent Metainference's Outliers model<sup>18</sup>. In the limit of  $\beta \rightarrow \infty$ , the likelihood becomes Gaussian. When considering the full posterior, this extra nuisance parameter is given a non-informative Jeffreys prior,  $p(\beta) \sim \beta^{-1}$ . For more details regarding the Student's model, see Figures S1-S2.

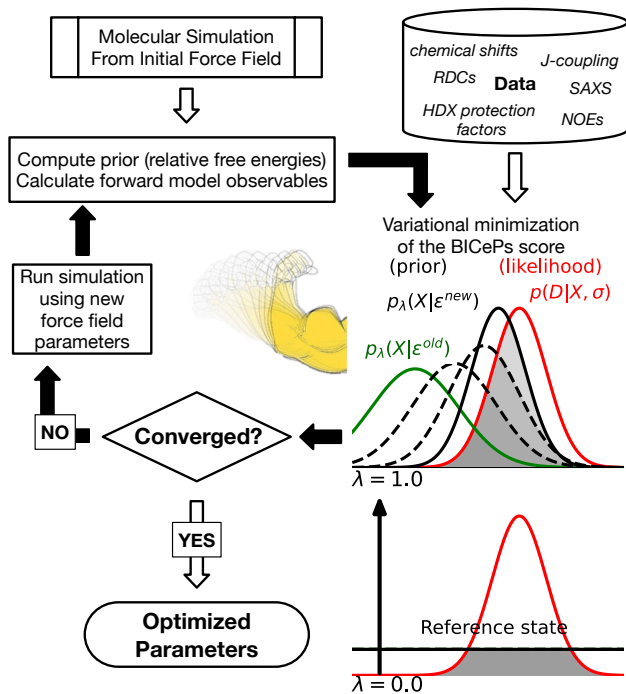


Figure 1. Force field optimization by variational minimization of the BICePs score. Given ensemble-averaged experimental observables  $D$ , and a simulated ensemble  $p_\lambda(X|\epsilon)$  generated from molecular simulation using initial force field parameters  $\epsilon$ , an automated procedure is used to find the optimal parameters  $\epsilon^*$  that best match experiment. The procedure is guided by the first and second derivatives of the BICePs score at each iteration to propose new values of  $\epsilon$ . optimal parameters  $\epsilon$ . This cycle is iterated until convergence is reached.

### B. The BICePs score: a tool for quantitative model selection and refinement

The BICePs score is a free energy-like quantity that rigorously characterizes model quality. For a model of prior populations  $p(X|\epsilon)$  parameterized by  $\epsilon$ , with corresponding prior energy  $E(X|\epsilon) = -\ln p(X|\epsilon)$ , the BICePs score  $f(\epsilon)$  is calculated as the negative logarithm of a Bayes factor,

$$f(\epsilon) = -\ln(Z(\epsilon)/Z_0). \quad (6)$$

$Z(\epsilon)$  is the total evidence of the specified model, marginalized over all conformational replicas and uncertainty. By defining the BICePs energy function as  $u = -\ln p(\mathbf{X}, \sigma|D, \epsilon)$ , it takes the form

$$Z(\epsilon) = \int \int \exp(-u(\mathbf{X}, \sigma | D, \epsilon)) d\mathbf{X} d\sigma, \quad (7)$$

$Z_0$  is defined similarly, but for a uniform prior that does not depend on  $\epsilon$ .  $Z_0$  thus serves as a well-defined reference state. By constructing a series of intermediates that scale the prior  $p_\lambda(X|\epsilon) \sim [p(X|\epsilon)]^\lambda$  as  $\lambda = 0 \rightarrow 1$ , the BICePs score is calculated as the change in free energy for “turning on” the prior (Figure 1).

### C. Variational minimization of the BICePs score to find optimal model parameters.

We assume there exists some posterior distribution  $p^*(\mathbf{X}, \sigma|D, \epsilon^*)$  with the maximal evidence, derived from optimal parameters  $\epsilon^*$ . In this case, the free energy  $f(\epsilon^*) = f^*$  is a global minimum, and any other set of parameters  $\epsilon$  has  $f(\epsilon) - f^* \geq 0$ .

Our objective is to find  $\epsilon^*$  starting with trial parameters  $\epsilon$  and corresponding distribution  $p(\mathbf{X}, \sigma|D, \epsilon)$ . To do this, we iteratively perform BICePs calculations  $\lambda = 0 \rightarrow 1$  to estimate  $f(\epsilon)$ , then update the parameters to further minimize this quantity, until the stopping criteria is reached. Given a differentiable prior,  $f(\epsilon)$  is also differentiable, enabling application of any number of gradient-based convex optimization schemes, with a stopping criteria of  $\left. \frac{\partial f}{\partial \epsilon} \right|_{\epsilon=\epsilon^*} = 0$ , within some tolerance.

The derivative of the BICePs score with respect to parameters  $\epsilon$  reduces to the ensemble-averaged value of  $\partial u / \partial \epsilon_i$ ,

$$\frac{\partial f}{\partial \epsilon_i} = \iint \frac{1}{Z(\epsilon)} \left[ \frac{\partial u}{\partial \epsilon_i} \right] \exp(-u) d\mathbf{X} d\sigma = \left\langle \frac{\partial u}{\partial \epsilon_i} \right\rangle, \quad (8)$$

where

$$\frac{\partial u}{\partial \epsilon_i} = \sum_{r=1}^N \left\{ \frac{\partial E(X_r|\epsilon)}{\partial \epsilon_i} - \left\langle \frac{\partial E(\mathbf{X}|\epsilon)}{\partial \epsilon_i} \right\rangle \right\} \quad (9)$$

The reference ensemble  $Z_0$  does not affect the gradient of  $f$ , since a uniform prior is independent of  $\epsilon$ , and  $\langle \partial u_0 / \partial \epsilon \rangle$  is zero (see section V for more details).

The second partial derivatives of the BICePs score with respect to parameters  $\epsilon_i$  and  $\epsilon_j$  are:

$$\begin{aligned} \frac{\partial^2 f(\epsilon)}{\partial \epsilon_i \partial \epsilon_j} = & \left\langle \frac{\partial^2 u}{\partial \epsilon_i \partial \epsilon_j} \right\rangle - \left( \left\langle \left( \frac{\partial u}{\partial \epsilon_i} \right) \left( \frac{\partial u}{\partial \epsilon_j} \right) \right\rangle \right. \\ & \left. - \left\langle \left( \frac{\partial u}{\partial \epsilon_i} \right) \right\rangle \left\langle \left( \frac{\partial u}{\partial \epsilon_j} \right) \right\rangle \right), \end{aligned} \quad (10)$$

where the notation  $\langle \cdot \rangle'$  denotes the ensemble average with respect to  $(\frac{1}{Z} \exp(-u))^2$ . The first term on the right is the ensemble-averaged second derivative of the energy function  $u$  with respect parameters  $\epsilon_i$  and  $\epsilon_j$ :

$$\begin{aligned} \frac{\partial^2 u}{\partial \epsilon_i \partial \epsilon_j} = & \sum_{r=1}^N \left\{ \frac{\partial^2 E(X_r|\epsilon)}{\partial \epsilon_i \partial \epsilon_j} - \left\langle \frac{\partial^2 E(\mathbf{X}|\epsilon)}{\partial \epsilon_i \partial \epsilon_j} \right\rangle \right. \\ & + \left\langle \left( \frac{\partial E(\mathbf{X}|\epsilon)}{\partial \epsilon_i} \right) \left( \frac{\partial E(\mathbf{X}|\epsilon)}{\partial \epsilon_j} \right) \right\rangle \\ & \left. + \frac{\sum_X \exp(-2E(X|\epsilon)) \left( \frac{\partial E(\mathbf{X}|\epsilon)}{\partial \epsilon_i} \right) \left( \frac{\partial E(\mathbf{X}|\epsilon)}{\partial \epsilon_j} \right)}{(\sum_X \exp(-E(X|\epsilon)))^2} \right\}. \end{aligned} \quad (11)$$

When  $i = j$ , the second partial derivative of the BICePs score reduces to the difference between the ensemble-averaged second derivative of the energy  $u$  and the variance of its first partial derivative:

$$\frac{\partial^2 f}{\partial \epsilon^2} = \left\langle \frac{\partial^2 u}{\partial \epsilon^2} \right\rangle - \left( \left\langle \left( \frac{\partial u}{\partial \epsilon} \right)^2 \right\rangle - \left\langle \frac{\partial u}{\partial \epsilon} \right\rangle^2 \right) \quad (12)$$

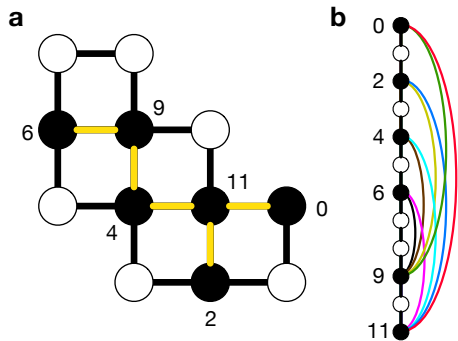


Figure 2. (a) The folded state of the 12-mer HP lattice model protein with sequence HPHPHPHPPHPH. Highlighted in yellow are the favorable non-bonded contacts between the hydrophobic residues (black beads). (b) Extended diagram of the eight distance measurements used in this work.

In practice, all of these quantities are estimated as ensemble-averaged observables at the same time  $f(\varepsilon)$  is estimated, using the MBAR free energy estimator. MCMC sampling at several intermediates  $\lambda = 0 \rightarrow 1$  enables accurate estimates of all quantities (Figure 1).

### III. METHODS

#### A. A toy protein lattice model

The HP lattice model of Dill and Chan<sup>20</sup> is a simplified protein folding model that represents a protein sequence as a chain of beads on a 2-D square lattice. In this model, each amino acid residue is classified as either a hydrophobic (H) or polar (P) bead. Each microscopic chain conformation  $X$  has an energy  $V(X)$  proportional to the number of H-H contacts  $n(X)$ ,

$$V(X) = -\varepsilon \cdot n(X), \quad (13)$$

A “contact” is defined as a non-sequential pair of hydrophobic residues at adjacent lattice sites. As a test system, we consider a 12-mer protein sequence HPHPHPHPPHPH (Figure 2a). When  $\varepsilon$  is sufficiently large, there is a single lowest-energy microstate that corresponds to the global free energy minimum; such sequences are deemed *foldable*. For the 12-mer HPHPHPHPPHPH sequence, there are 15037 unique microstate conformations that can be binned into 72 macrostates, each with a unique set of contacts.

To explore a system with multiple parameters, we modify the HP model to include multiple interactions. Each bead with sequence position  $i$  is assigned a unique interaction strength,  $\varepsilon_i$ , and a geometric-average combination rule is used to compute the energy  $V$  of each microstate:

$$V = \sum_{i,j \text{ in contact}} -(\varepsilon_i \varepsilon_j)^{1/2}, \quad (14)$$

where the sum is taken over all pairs of residues  $(i, j)$  that are in contact.

The first derivative of the contact energy with respect to  $\varepsilon_i$  is given by

$$\frac{\partial V}{\partial \varepsilon_i} = \sum_{i,j \text{ in contact}} -\frac{1}{2}(\varepsilon_i \varepsilon_j)^{-1/2} \varepsilon_j, \quad (15)$$

and the second derivative of the contact energy with respect to  $\varepsilon_i$  and  $\varepsilon_j$  is given by:

$$\frac{\partial^2 V}{\partial \varepsilon_i \partial \varepsilon_j} = \sum_{i,j \text{ in contact}} \frac{1}{4}(\varepsilon_i \varepsilon_j)^{-3/2} \varepsilon_j \varepsilon_i. \quad (16)$$

We use the 72 macrostates with unique contacts as a set of prior populations for use with BICePs. For each macrostate  $k$ , the populations  $p_k$  are computed as

$$p_k = \frac{g_k \exp(-V_k)}{\sum_k g_k \exp(-V_k)}, \quad (17)$$

where  $V_k$  is the reduced energy (in units  $k_B T$ ) of each microstate in macrostate  $k$ , and  $g_k$  is the multiplicity (the number of microstates belonging to macrostate  $k$ ).

The ensemble-averaged distance observables for each macrostate (and their variance over all microstates belonging to it) are computed as follows. Let  $(d_{ij})_k$  represent the average distance between residues  $i$  and  $j$  in the  $k^{\text{th}}$  macrostate. Then, the ensemble-averaged distance observables are given by:

$$\langle d_{ij} \rangle = \sum_k p_k (d_{ij})_k, \quad (18)$$

and the variance of the distance observables is given by:

$$\sigma^2(\langle d_{ij} \rangle) = \sum_k p_k^2 \sigma^2((d_{ij})_k), \quad (19)$$

where  $\sigma^2((d_{ij})_k)$  is the variance of the average distance between residues  $i$  and  $j$  in the  $k^{\text{th}}$  macrostate.

For ease of interpretation, we assume that the distance units of the square lattice are Ångstroms ( $1\text{Å} = 10^{-10} \text{ m}$ ).

### IV. RESULTS AND DISCUSSION

#### A. The BICePs score landscape correctly identifies optimal parameters for an HP lattice model.

To understand BICePs’ ability to learn optimal parameters, we start by scanning the BICePs score landscape over a single  $\varepsilon$  parameter. For this purpose, we use an HP model where all six hydrophobic beads share the same value of  $\varepsilon_i = \varepsilon$ .

To generate a set of experimental distance observables for testing, we set the “true” value of  $\varepsilon$  to 1.0., and compute average distances and variances of eight distances for each macrostate (Figure 2b). The BICePs score and its first and second derivatives are then evaluated across a range of  $\varepsilon$  values, spanning from 0.0 to 5.5, in increments of 0.125, where prior energies are unique for each  $\varepsilon$  value. BICePs scores and derivatives are averaged over five independent calculations using 100k steps of MCMC with 8 replicas. The associated error

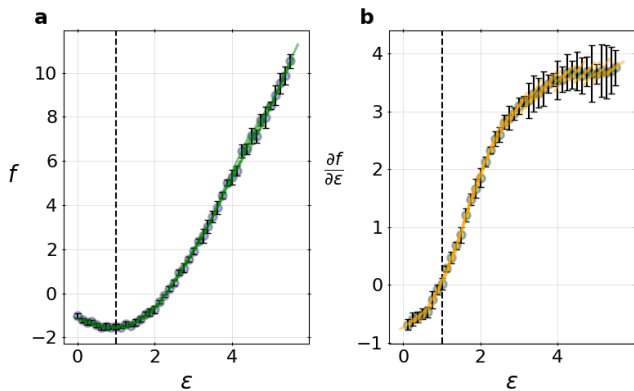


Figure 3. (a) 1-D scans over  $\epsilon$  to reveal the landscape of the BICePs score (blue dots). The green tangent lines are the computed derivatives at each  $\epsilon$  value. Uncertainties in the BICePs scores and their derivatives come from five independent scans along  $\epsilon$ . (b) The derivative of the BICePs score (blue dots) and the second derivative of the BICePs score (yellow lines) at each epsilon value. The dotted black line at  $\epsilon = 1.0$  shows the true value, which is where the derivative of the BICePs score equals zero. BICePs calculations are run using the Student’s model for 100k steps with 8 replicas.

bars represent the standard error of the mean across these five instances.

The resulting  $f(\epsilon)$  landscape pinpoints the optimal parameter as a minimum, and correctly computes the first and second derivatives (Figure 3). Despite the stochastic sampling inherent to BICePs, the BICePs score landscape is remarkably smooth and precise, revealing the optimal epsilon to be  $\epsilon^* = 1.0$ , the value with the lowest BICePs score,  $f(\epsilon^*)$  (Figure 3a.), with its derivative  $df/d\epsilon$  at this location equal to 0.0 (Figure 3b.). This optimal model is achieved when the overlap between the likelihood and prior distributions is maximized (Figure 1). When  $\epsilon$  is significantly larger than the true value, the uncertainty in  $f$  and  $\partial f/\partial\epsilon$  increases. In this case, the physical interpretation is that for large values of  $\epsilon$  the 12-mer primarily populates the folded macrostate, which results in poor overlap between the likelihood and prior, and more finite sampling error.

## B. Automated optimization schemes.

With the ability to compute first and second derivatives of the BICePs score, we next explored the performance of automated optimization methods L-BFGS-B<sup>21</sup> and Trust-NCG<sup>22</sup> on the single- $\epsilon$  system. L-BFGS-B is a first-order approach that uses information from gradients, while Trust-NCG is a second-order approach that additionally makes use of information from the Hessian. All default optimization parameters from SciPy were used except a value of  $\text{ftol}=1\text{e-}8$  (default:  $\text{ftol}=1\text{e-}9$ ), and the bounds for each parameter to be optimized was set to be in the range  $[0, 10]$ . With only a single parameter, automatic refinement using both optimization methods quickly finds the minimum in a single iteration (Fig-

ure S3). However, use of the Hessian (second-order) enables faster convergence, and tends to be slightly more robust for this particular example.

## C. The Student’s model confers resiliency when dealing with experimental error.

We next examined the robustness of the BICePs score to errors and uncertainties present in experimental data, by introducing random and systematic errors to the 2–11 and 0–11 distance observables (Figure S4). When we used BICePs with a standard Gaussian likelihood model in which a single uncertainty parameter  $\sigma$  is used for all experimental observables, introducing random and systematic errors significantly reduces the accuracy of the model. When 2–11 and 0–11 distances are perturbed by +3 to +5 Å, the BICePs score predicts a value of  $\epsilon$  smaller than the “true” value, predicting structures that are primarily “unfolded”. This in turn causes a leftward shift in the gradient plot (Figure 3b).

In contrast, the Student’s likelihood model deals with the outliers much more handily. The minimum BICePs score correctly identifies the optimal value of  $\epsilon$ , and the leftward shift in the gradient plot is absent. The Student’s model is able to automatically identify outliers directly from the input data, and mitigate their influence, even when 25% of the data (2 of the 8 distances) are corrupted.

To more critically assess the performance of the Gaussian and Student’s models in dealing with systematic errors, we examine the extent to which the gradient of the BICePs score deviates from zero at the “true” value of  $\epsilon^* = 1$ . We introduced random perturbations to the 2–11 and 0–11 distances of various standard deviations,  $\sigma_{data}$  (Figure 4). When the Gaussian likelihood model was used, the computed gradient at  $\epsilon^* = 1$  increases proportionally with the magnitude of  $\sigma_{data}$ , and becomes particularly unreliable when the error surpasses 0.75 Å. When the Student’s model was used, however, we find that such deviations are reduced. As  $\sigma_{data}$  increases from zero, the gradient at  $\epsilon^* = 1$  begins to increase, but then begins to decrease beyond  $\sigma_{data} = 0.6$  Å. This happens because the perturbations in the distance observables become large enough to be detected as outliers by the Student’s model.

## D. Multiparameter optimization

While our toy protein lattice model is very simple, the inference problem it presents is challenging, especially as we increase the number of epsilon parameters to refine. Our 12-mer system has only eight experimental distances as experimental restraints, and these are significantly influenced by ensemble-averaging. Moreover, the protein lattice model has a highly cooperative folding landscape, which can lead to correlated distance restraints that don’t independently provide informative insights.

With this in mind, we further tested multi-parameter minimization of the BICePs score, using the modified HP lattice

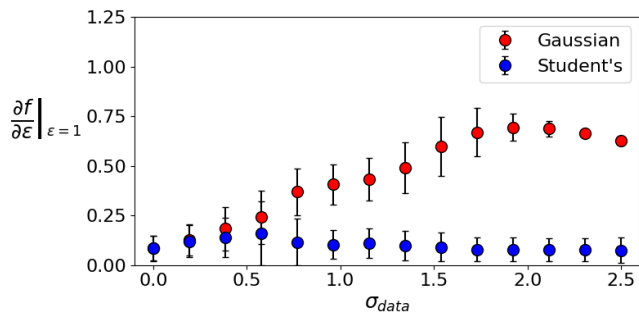


Figure 4. Comparative analysis in performance of the Student’s likelihood model (blue) and a Gaussian likelihood model (red), when random and systematic error of varying magnitude ( $\sigma_{data}$ ) is introduced to the 2-11 and 0-11 distances. The vertical axis shows the derivative of the BICePs score evaluated at the “true” target value,  $\epsilon = 1$ . This value corresponds to the “True” minima, illustrated in Figure 3. The Gaussian likelihood’s derivative becomes notably less dependable when data incorporates errors, especially when  $\sigma_{data}$  exceeds 0.75, surpassing one standard deviation. The values shown were calculated using 5000 random perturbations to the 2-11 and 0-11 distances, and represent the average of 300 BICePs calculations. Error bars represent the standard deviation.

model with tunable interaction strengths  $\epsilon_i$ . Ideally, our algorithm should be able to efficiently find the global minimum of  $f(\epsilon_1, \epsilon_2, \dots)$  starting from many different initial parameter sets, and be resilient against random and systematic errors. For two or more  $\epsilon_i$  parameters, it becomes computationally expensive to perform multidimensional scans of the BICePs score landscape, necessitating automated parameter optimization.

We first generated test data for a model where we set the “true” values to  $\epsilon_2 = 1.25$ ,  $\epsilon_4 = 1.5$  and the remaining  $\epsilon_i$  set to 3.0. We then tested two-parameter ( $\epsilon_2, \epsilon_4$ ) optimizations, starting from three different initial parameter sets  $(\epsilon_2^0, \epsilon_4^0) = \{(0.5, 5.0), (4.0, 5.0), (4.0, 0.5)\}$ , using both L-BFGS-B and ‘trust-ncg’ optimization for BICePs scores calculated using 8 replicas. Optimizations using L-BFGS-B are unable to fully reach the “true” values of the interaction strength parameters ( $\epsilon_2^{\text{True}} = 1.25$ ,  $\epsilon_4^{\text{True}} = 1.5$ ) within 10 iterations (Figure S5). The ‘trust-ncg’ optimization, however, successfully found the correct minima within 10 iterations, demonstrating the notable advantage of second-order methods (Figure S6).

To visualize the two-parameter BICePs score landscape  $f(\epsilon_2, \epsilon_4)$ , we constructed a smooth 2-D landscape by averaging five repeated evaluations over a  $(6 \times 6)$  set of grid points, and trained a Gaussian process regression on the grid values using an RBF kernel. The landscape matches the computed BICePs scores, and shows that trajectories of successive  $(\epsilon_2, \epsilon_4)$  values correctly follow gradients, normal to the landscape contour lines.

The reported uncertainties in the optimized  $(\epsilon_2, \epsilon_4)$  values comes from an estimation of the covariance through inversion of the Hessian (the matrix of second partial derivatives of the BICePs score):

$$\sigma_\epsilon = \sqrt{\text{diag}[\mathbf{H}^{-1}]}. \quad (20)$$

Conceptually, this means that the estimated uncertainties in the best-fit values represent the widths of the basins on the BICePs score landscape. This can sometimes lead to an overestimation of the uncertainty with trust-region optimization schemes, especially with flatter basins like those we observe in the BICePs score landscape. Conversely, the sharper the curvature (larger eigenvalues of the Hessian), the more certain we are about the location of the minimum in that direction, resulting in smaller computed uncertainties. Inspection of Equations (9), (12) and (A16) show that  $\sigma_\epsilon \propto 1/\sqrt{N}$ , where  $N$  is the number of BICePs replicas. This suggests that one can obtain smaller uncertainties in the optimized parameters by using more replicas (albeit at greater computational expense). Indeed, repeating the ‘trust-ncg’ optimization with 32 BICePs replicas results in average optimized parameters of  $\epsilon_2 = 1.12 \pm 0.39$ , and  $\epsilon_4 = 1.43 \pm 0.34$ , which have smaller uncertainty estimates compared to the calculations made with 16 replicas ( $\sigma_{\epsilon_2} = 0.59$ , and  $\sigma_{\epsilon_4} = 0.47$ ). (Figure S7).

In all our multiparameter optimizations, we use a standardized convergence criterion, determined by assessing the average relative change between the old parameters  $\epsilon_i^{\text{old}}$  and the new parameters  $\epsilon_i^{\text{new}}$  at each iteration, calculated as

$$\frac{1}{N_\epsilon} \sum_{i=1}^{N_\epsilon} \left| \frac{\epsilon_i^{\text{old}} - \epsilon_i^{\text{new}}}{\epsilon_i^{\text{old}}} \right| < 0.05, \quad (21)$$

where convergence is considered to have been reached when the average change in parameters is less than 0.05. In addition, we strictly require that the convergence condition is satisfied three times in succession.

### E. Multiparameter optimization in the presence of systematic error

To assess the resiliency of multiparameter optimization to systematic error, we added extra complexity to the optimization problem by introducing systematic error of +3 Å and +3.5 Å to the 2–11 and 4–9 distances observables, respectively. This makes total error in the data  $\sigma_{data} = 1.63$  Å, a significant obstacle to the refinement of parameters  $\epsilon_2$  and  $\epsilon_4$ , considering these beads each participate in only two of measured distances (Figure 2b).

We performed ‘trust-ncg’ optimization using the Student’s model with 200k MCMC steps and 32 replicas, starting from three different initial parameters:  $(\epsilon_2^0, \epsilon_4^0) = \{(0.5, 5.0), (4.0, 5.0), (4.0, 0.5)\}$  (Figure 5). Indeed, repeating the ‘trust-ncg’ optimization with 32 BICePs replicas results in average optimized parameters of  $\epsilon_2 = 1.24 \pm 0.41$ , and  $\epsilon_4 = 1.31 \pm 0.33$ , which have smaller uncertainty estimates compared to the calculations made with 16 replicas ( $\epsilon_2 = 1.28 \pm 0.59$ , and  $\epsilon_4 = 1.31 \pm 0.47$ ). Notably, this was achieved in only a few iterations, showing the algorithm’s proficiency in finding the optimal parameters, irrespective of the initial reference parameters.

In adherence to best practices<sup>23</sup>, we compute accuracy profiles for two-parameter ‘trust-ncg’ optimizations using 32 BICePs replicas with no systematic error (Figure S8) and sys-

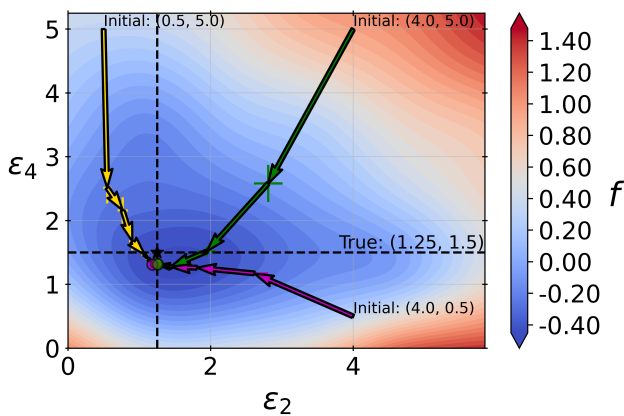


Figure 5. Average traces over a total of 25 independent rounds of parameter  $(\epsilon_2, \epsilon_4)$  optimizations using second-order (trust-ncg) method with BICePs, for a maximum of ten iterations. Optimizations converge to the same parameters  $(\epsilon_2^{\text{True}} = 1.25, \epsilon_4^{\text{True}} = 1.5)$  when starting from different initial parameters  $(\epsilon_2^0, \epsilon_4^0) = \{(0.5, 5.0), (4.0, 5.0), (4.0, 0.5)\}$ . Average BICePs optimized parameters were determined to be  $\epsilon_2 = 1.24 \pm 0.41$ , and  $\epsilon_4 = 1.31 \pm 0.33$ , where the uncertainties are estimated from the inverse Hessian. The BICePs score landscape was generated from the average values of five scans over  $\epsilon_2$  and  $\epsilon_4$ . All calculations used the Student’s model with 200k MCMC steps and 32 replicas. The experimental data is corrupted with systematic error in the 2-11 and 4-9 distances for +3 and +3.5Å shift, respectively. The total error in the data is  $\sigma_{data} = 1.63$ .

tematic error (Figure S9). The accuracy profiles show the relative error  $\|\vec{\epsilon} - \epsilon^*\|_2 = \sqrt{\sum_i (\epsilon_i - \epsilon_i^*)^2}$  as a function of number of iterations. Optimizations with no systematic error were repeated using only 16 BICePs replicas (Figure S10). A comparison of the 16-replica and 32-replica results shows that the variance between independent optimization traces decreases as the number of replicas increases. The error bars plotted in the accuracy profiles report uncertainties estimated from the inverse Hessian. In each case, it can be seen that the actual variation in the relative error across many optimizations is well within the Hessian-estimated uncertainty.

As we did with the one-parameter optimizations, we also examined the performance of two-parameter optimizations when using a standard Gaussian likelihood model, in the absence of systematic error (Figure S11a) and in the presence of systematic error (Figure S11b). As before, we find that the accuracy of the refined parameters drops significantly when using a standard Gaussian likelihood model. With only a single parameter to estimate the uncertainty in the data set of distances, the Gaussian likelihood model is unable to properly detect the two outliers, and as a result predicts optimal  $\epsilon_2$  and  $\epsilon_4$  values that are much smaller than the “true” values. Conversely, the accuracy of the Student’s model is very robust in the presence of systematic error (Figure S12). These results yet again highlight the ability of BICePs to handle uncertainties and systematic error comprehensively when used with a likelihood model that can deal with outliers.

## F. Performance in higher-dimensional parameter landscapes

We next attempted to optimize a three-parameter BICePs score landscape, by introducing an additional parameter,  $\epsilon_6$ . This is a challenging task that may take many iterations to reach the convergence criteria. Our objective was to examine the typical percentage of optimization traces that converge within a designated number of iterations. For this test, we refrained from adding systematic error to the data.

Five initial starting points were selected:  $(\epsilon_2^0, \epsilon_4^0, \epsilon_6^0) = (4.0, 5.0, 3.0), (0.5, 5.0, 0.5), (2.0, 4.0, 4.0), (1.0, 0.5, 3.0), (3.0, 0.5, 0.5)$ . Optimization targeted the “true” interaction strength parameters:  $\epsilon_2^{\text{True}} = 1.25, \epsilon_4^{\text{True}} = 1.5$ , and  $\epsilon_6^{\text{True}} = 1.5$ , with an acceptable average relative deviation of 0.2 (refer to Figure 6). Twenty-five independent optimizations were performed per starting point, using 32 BICePs replicas and 200k MCMC steps per iteration.

For these tests, we required that the convergence condition must be satisfied two times in succession, which is a typical stopping point. Traces of the relative error throughout the optimization show a heterogeneous collection of convergence trajectories, depending on the starting point (Figure 6). At each iteration, we track the percentage of traces that remain unconverged. For some starting points, all optimization trajectories converge within ten iterations, while for others, up to 28% remain unconverged going into the tenth iteration. The average optimized parameters from the converged trajectories were determined to be  $(\epsilon_2 = 1.17 \pm 0.38, \epsilon_4 = 1.37 \pm 0.32, \epsilon_6 = 1.51 \pm 0.37)$ , where the uncertainties are calculated from the inverse Hessian. An overlay of average traces on the BICePs score landscape is shown in Figure S13.

A robust correlation ( $R^2 = 0.96$ ) between the converged BICePs score and the relative error in the parameters further confirms the validity of our approach in higher dimensions (see Figure S14). This relationship illustrates that an increased distance from the “true” parameters (i.e. a higher relative error) corresponds to an enlargement of the BICePs score  $f$ . A comparative analysis of average BICePs scores across optimization traces (Figure S15) and the landscape contours (Figure S13) indicates that our Gaussian process regression does a fine job of approximating the actual BICePs score landscape in higher dimensions.

## G. Köfinger & Hummer’s toy polymer model

Köfinger and Hummer (KH) recently developed a method to optimize molecular simulation force fields using a Bayesian inference maximum-entropy reweighting method called BioFF.<sup>3</sup> To validate their method, they introduced a simple parameterizable 2-D polymer model, and demonstrated that BioFF can efficiently discover the optimal parameters that reproduce ensemble-averaged observables. Here, we demonstrate that BICePs optimization can also reproduce this result.

The KH polymer model is a chain of  $N$  beads, each separated by unit length, with orientations defined by  $N - 1$  angles  $\Delta\phi$  between contiguous bond vectors. Each bond angle is dis-

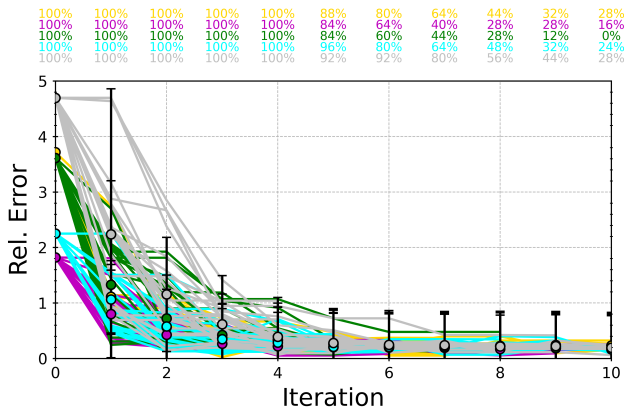


Figure 6. Accuracy profile of optimization traces, demonstrating convergence with a relative error of 0.2. A total of 25 independent rounds of parameter ( $\epsilon_2, \epsilon_4, \epsilon_6$ ) optimizations were conducted for each of the five sets of initial parameters ( $\epsilon_2^0, \epsilon_4^0, \epsilon_6^0$ ): (4.0, 5.0, 3.0) (gray), (0.5, 5.0, 0.5) (yellow), (2.0, 4.0, 4.0) (green), (1.0, 0.5, 3.0) (magenta), (3.0, 0.5, 0.5) (cyan). Color-coded percentages report the fraction of trajectories that remain unconverged at each iteration. Error bars (black) represent the uncertainties in predicted parameters for each iteration, calculated using the diagonalized inverse Hessian (Equation (20)) and averaged over the 25 independent optimizations. Average optimized parameter values from converged trajectories were ( $\epsilon_2 = 1.17 \pm 0.38, \epsilon_4 = 1.37 \pm 0.32, \epsilon_6 = 1.51 \pm 0.37$ ).

tributed according a von Mises distribution parameterized by  $\kappa$ , which controls the polymer’s stiffness. Full details about this model are given in Appendix B. Unlike the HP lattice model, which possesses an exact solution for the prior, the KH polymer model requires estimation of the prior through statistical sampling, which is subject to finite sampling error.

To implement KH model optimization with BICePs, we derived the first and second partial derivatives of the energy function required for computation of the BICePs score (see SI). Following Köfnger and Hummer, we consider a 100-bead chain, and use the end-to-middle distance (between bead 1 and bead 50) as the ensemble-averaged observable, which we estimate as the mean of 10000 samples from the von Mises distribution with the “true” value of  $\kappa$  set to 10.0.

We then performed ‘trust-ncg’ optimization using 200 BICePs replicas and 100k MCMC steps, starting from an initial parameter value of  $\kappa = 20.0$ . At the first optimization step, draw 500 samples from the von Mises distribution, and use their energies to compute their Boltzmann populations; each sample is a separate conformational state. In each subsequent optimization step, we draw 500 more samples to add to the collection, and compute energies and Boltzmann populations for the combined collection. The result of this procedure is highly efficient discovery of the optimal value of  $\kappa^* = 10$ , reaching convergence within two iterations (Figure S16).

While BICePs optimization achieves similar results to BioFF, it is worth mentioning some of the key differences of the two methods. BioFF is a maximum-entropy method that reweights a set of reference populations by minimizing a negative log-likelihood that uses a regularization parameter,

$\theta$ , to balance two terms: the relative entropy with respect to the reference, and a  $\chi^2$  term representing the deviation between model predictions of ensemble-averaged quantities and experiment. The BioFF-based optimization algorithm iteratively (1) reweights the populations given a current set of force field parameters, then (2) optimizes the force field parameters given the updated populations, repeating this cycle until convergence.

One issue with this approach is that it requires a coarse-grained description of the relevant conformational states and their populations, which need to be revised as the force field parameters are optimized. Köfnger and Hummer deal with this by keeping track of each new thermodynamic ensemble being sampled, and using the running collection of all the samples obtained to estimate each new set of coarse-grained state populations with the binless WHAM<sup>24,25</sup> free energy estimator. In our BICePs approach, we avoid this expense by simply adding new samples as additional conformational states, and recalculating populations as their Boltzmann weights.

Another issue with maximum-entropy methods like BioFF<sup>3,26</sup> and BioEn<sup>27</sup> is the need to choose an appropriate value for the regularization parameter  $\theta$ . BICePs does not require a regularization parameter, because the BICePs score is computed by sampling the entire posterior distribution of uncertainty parameters  $\sigma$ . (In BICePs, the  $\sigma$  are the analogous quantities that balance prior information against the experimental restraints.)

Very recently, Köfnger & Hummer put the regularization parameter  $\theta$  on a firmer theoretical footing by relating it to the variance of the reduced energy difference, thus enabling estimation of  $\theta$  *a priori*.<sup>28</sup> Another recent work, Gilardoni et al.<sup>29</sup> introduced an approach similar to BICePs, in that ensemble refinement and force field parameter refinement are integrated into a singular process. This method bears resemblance to both BioEn and BioFF, as it employs a regularization parameter to scale the Kullback-Leibler divergence. Gilardoni et al.’s technique is distinguished by the incorporation of two distinct confidence hyperparameters. The first parameter is designed to adjust the reliability of the prior, while the second modulates the trustworthiness of the force field corrections.

## H. Further Discussion

Our work here greatly improves upon previous work by Ge et al., which used an HP lattice model as an example system to perform force field parameterization and model selection using BICePs.<sup>5</sup> That work approached the problem through brute force, scanning parameter space in search of the minimum BICePs score, which would be costly and impractical for multiple parameters. Another issue with that work was the use of a previous version of BICePs (called BICePs v1.0) that does not use replica-averaging, and therefore was not a maximum-entropy method. Because of this, applying BICePs in practical cases, such as refining conformational populations against NMR observables for beta-hairpins trploop 2A and 2B, resulted in ensembles dominated by the state(s) that best

agree with experiment. Since that work, we have developed the current version of BICePs that performs replica averaging and is equipped with specialized likelihood functions that can account for systematic error.<sup>12</sup> The HP lattice model continues to serve as an excellent test system for force field refinement as it grants the option to use multiple parameters and provides exact solutions for generated ensembles.

While our algorithm has the advantage of being able to incorporate priors on force field parameters, this is a possibility we do not pursue in this work. Obtaining priors for force field parameters is a more involved approach, but we leave room for this in future development.

### I. Optimization across multiple systems

An eventual application of our BICePs optimization method is transferable force field parameterization across many different molecular systems (e.g. a set of proteins) against ensemble-averaged experimental measurements.

Our approach can easily be adapted for this purpose, and performed efficiently so that each molecular system can be evaluated in a separate BICePs calculation. To do this, suppose we have a set of molecular systems indexed by  $s$ , of total number  $N_s$ . We make use of the partial derivatives of the BICePs score with respect to each  $\epsilon_i$  to determine a weight for each system  $s$ . The normalized weight for the  $i^{\text{th}}$  parameter of system  $s$  is

$$w_{i,s} = \frac{\left(\frac{\partial f}{\partial \epsilon_i}\right)_s (\epsilon_{i,s} - \epsilon_i^{\text{old}})}{\sum_{s=1}^{N_s} \left(\frac{\partial f}{\partial \epsilon_i}\right)_s (\epsilon_{i,s} - \epsilon_i^{\text{old}})}. \quad (22)$$

At each optimization iteration, we update the  $i^{\text{th}}$  parameter,  $\epsilon_i^{\text{new}}$  according to a weighted average across all of the systems:

$$\epsilon_i^{\text{new}} \leftarrow \sum_{s=1}^{N_s} w_{i,s} \epsilon_{i,s}. \quad (23)$$

In this scheme, the derivatives play a pivotal role, where the weights are determined by how significantly each parameter change influences the BICePs score. This provides a balance, ensuring parameters from a system with larger effects on the score have more influence in determining the next set of parameters  $\epsilon_{\text{new}}$ .

### J. Outlook

Looking ahead, there is tremendous potential to extend the scope of the BICePs optimization against ensemble averaged observables to many applications. One area of application would be to optimize physics-based molecular mechanics force fields for proteins against the many published solution-NMR data that exists.<sup>30</sup> Another application would be to optimize parameters of general-purpose force fields for bespoke applications. Examples of this may include refining

existing all-atom microscopic models to better predict macroscopic properties (e.g. ensemble-average properties of disordered peptides like radius of gyration), or developing classes of models that can better predict the experimental observables for peptidomimetics without having to perform expensive fitting to quantum mechanical energy surfaces. In principle, any parameterizable model for the prior can be used with BICePs, including neural-network based potentials, or even generative models obtained from deep learning methods.

## V. CONCLUSION

In this work, we showed how the BICePs approach can be used for automatic and robust optimization of force field parameters against ensemble-averaged experimental measurements. This is done by variational minimization of the BICePs score, a free energy-like quantity characterizing how well a model agrees with the experimental data, calculated by sampling over the posterior distribution of possible uncertainties. Using information from first and second partial derivatives of the BICePs score with respect to model parameters, we show how robust multi-parameter optimization of the BICePs score can be performed. Demonstrations in simple toy protein lattice models and polymer models show the utility of the method, and how specialized likelihood functions to deal with outliers are especially good at dealing systematic error. These results suggest automated variational optimization of the BICePs score is a powerful approach for the parameterization of molecular potentials.

## CONFLICTS OF INTEREST

Authors declare no conflicts of interest.

## DATA AND SOFTWARE

The BICePs algorithm is freely available at [github.com/vvoelz/biceps](https://github.com/vvoelz/biceps) and can be installed using `pip install biceps`. The HP lattice model is open source software, located at: [github.com/vvoelz/HPSandbox](https://github.com/vvoelz/HPSandbox). All data, scripts, Jupyter notebook examples and analysis can be found here: [github.com/robraddi/biceps\\_FFOpt](https://github.com/robraddi/biceps_FFOpt). Detailed documentation and tutorials can be found here: <https://biceps.readthedocs.io>. For any issues or questions, please submit the request on GitHub.

## ACKNOWLEDGEMENTS

RMR and VAV are supported by National Institutes of Health grant R01GM123296.

## REFERENCES

- <sup>1</sup>S. Boothroyd, P. K. Behara, O. C. Madin, D. F. Hahn, H. Jang, V. Gapsys, J. R. Wagner, J. T. Horton, D. L. Dotson, M. W. Thompson, *et al.*, "Development and benchmarking of open force field 2.0. 0: The sage small molecule force field," *Journal of Chemical Theory and Computation* (2023).
- <sup>2</sup>J. S. Smith, B. T. Nebgen, R. Zubatyuk, N. Lubbers, C. Devereux, K. Barros, S. Tretiak, O. Isayev, and A. E. Roitberg, "Approaching coupled cluster accuracy with a general-purpose neural network potential through transfer learning," *Nature communications* **10**, 2903 (2019).
- <sup>3</sup>J. Köfinger and G. Hummer, "Empirical Optimization of Molecular Simulation Force Fields by Bayesian Inference," *The European Physical Journal B* **94**, 245 (2021).
- <sup>4</sup>L.-P. Wang, T. J. Martinez, and V. S. Pande, "Building Force Fields: An Automatic, Systematic, and Reproducible Approach," *The journal of physical chemistry letters* **5**, 1885–1891 (2014).
- <sup>5</sup>Y. Ge and V. A. Voelz, "Model Selection Using BICePs: a Bayesian Approach for Force Field Validation and Parameterization," *J. Phys. Chem. B* **122**, 5610–5622 (2018).
- <sup>6</sup>O. C. Madin, S. Boothroyd, R. A. Messerly, J. Fass, J. D. Chodera, and M. R. Shirts, "Bayesian-Inference-Driven Model Parametrization and Model Selection for 2CLJQ Fluid Models," *J. Chem. Inf. Model.* **62**, 874–889 (2022).
- <sup>7</sup>V. A. Voelz, Y. Ge, and R. M. Raddi, "Reconciling Simulations and Experiments with BICePs: a Review," *Front. Mol. Biosci.* **8**, 661520 (2021).
- <sup>8</sup>R. M. Raddi, T. Marshall, Y. Ge, and V. Voelz, "Model Selection Using Replica Averaging with Bayesian Inference of Conformational Populations," (2023).
- <sup>9</sup>V. a. Voelz and G. Zhou, "Bayesian Inference of Conformational State Populations from Computational Models and Sparse Experimental Observables," *J. Comput. Chem.* **35**, 2215–2224 (2014).
- <sup>10</sup>H. Wan, Y. Ge, A. Razavi, and V. A. Voelz, "Reconciling Simulated Ensembles of Apomyoglobin with Experimental Hydrogen/Deuterium Exchange Data Using Bayesian Inference and Multiensemble Markov State Models," *J. Chem. Theory Comput.* **16**, 1333–1348 (2020).
- <sup>11</sup>M. F. D. Hurley, J. D. Northrup, Y. Ge, C. E. Schafmeister, and V. A. Voelz, "Metal Cation-Binding Mechanisms of Q-Proline Peptoid Macrocycles in Solution," *J. Chem. Inf. Model.* **61**, 2818–2828 (2021).
- <sup>12</sup>R. M. Raddi, Y. Ge, and V. A. Voelz, "BICePs V2. 0: Software for Ensemble Reweighting Using Bayesian Inference of Conformational Populations," *Journal of chemical information and modeling* **63**, 2370–2381 (2023).
- <sup>13</sup>J. W. Pitera and J. D. Chodera, "On the Use of Experimental Observations to Bias Simulated Ensembles," *Journal of chemical theory and computation* **8**, 3445–3451 (2012).
- <sup>14</sup>A. Cavalli, C. Camilloni, and M. Vendruscolo, "Molecular Dynamics Simulations with Replica-Averaged Structural Restraints Generate Structural Ensembles According to the Maximum Entropy Principle," *The Journal of chemical physics* **138**, 03B603 (2013).
- <sup>15</sup>A. Cesari, S. Reißer, and G. Bussi, "Using the Maximum Entropy Principle to Combine Simulations and Solution Experiments," *Computation* **6**, 15 (2018).
- <sup>16</sup>B. Roux and J. Weare, "On the Statistical Equivalence of Restrained-Ensemble Simulations with the Maximum Entropy Method," *The Journal of chemical physics* **138**, 02B616 (2013).
- <sup>17</sup>G. Hummer and J. Köfinger, "Bayesian Ensemble Refinement by Replica Simulations and Reweighting," *The Journal of chemical physics* **143**, 12B634\_1 (2015).
- <sup>18</sup>M. Bonomi, C. Camilloni, A. Cavalli, and M. Vendruscolo, "Metainference: A Bayesian Inference Method for Heterogeneous Systems," *Sci. Adv.* **2**, e1501177 (2016).
- <sup>19</sup>D. Sivia and J. Skilling, *Data Analysis: a Bayesian Tutorial* (OUP Oxford, 2006).
- <sup>20</sup>K. A. Dill, S. Bromberg, K. Yue, H. S. Chan, K. M. Ftebig, D. P. Yee, and P. D. Thomas, "Principles of protein folding—a perspective from simple exact models," *Protein science* **4**, 561–602 (1995).
- <sup>21</sup>R. H. Byrd, P. Lu, J. Nocedal, and C. Zhu, "A limited memory algorithm for bound constrained optimization," *SIAM Journal on scientific computing* **16**, 1190–1208 (1995).
- <sup>22</sup>S. J. Wright, *Numerical optimization* (2006).
- <sup>23</sup>V. Beiranvand, W. Hare, and Y. Lucet, "Best Practices for Comparing Optimization Algorithms," *Optim. Eng.* **18**, 815–848 (2017).
- <sup>24</sup>M. R. Shirts and J. D. Chodera, "Statistically Optimal Analysis of Samples from Multiple Equilibrium States," *J. Chem. Phys.* **129**, 124105–11 (2008).
- <sup>25</sup>E. Rosta, M. Nowotny, W. Yang, and G. Hummer, "Catalytic mechanism of rna backbone cleavage by ribonuclease h from quantum mechanics/molecular mechanics simulations," *Journal of the American Chemical Society* **133**, 8934–8941 (2011).
- <sup>26</sup>J. Köfinger, B. Różycki, and G. Hummer, "Inferring Structural Ensembles of Flexible and Dynamic Macromolecules Using Bayesian, Maximum Entropy, and Minimal-Ensemble Refinement Methods," *Biomolecular Simulations: Methods and Protocols*, 341–352 (2019).
- <sup>27</sup>S. Bottaro, T. Bengtsen, and K. Lindorff-Larsen, "Integrating Molecular Simulation and Experimental Data: a Bayesian/Maximum Entropy Reweighting Approach," in *Structural Bioinformatics* (Springer, 2020) pp. 219–240.
- <sup>28</sup>J. Köfinger and G. Hummer, "Encoding prior knowledge in ensemble refinement," (2023).
- <sup>29</sup>I. Gilardoni, T. Fröhling, and G. Bussi, "Boosting ensemble refinement with transferable force field corrections: synergistic optimization for molecular simulations," arXiv preprint arXiv:2311.13532 (2023).
- <sup>30</sup>C. E. Cavender, D. A. Case, J. C.-H. Chen, L. T. Chong, D. A. Keedy, K. Lindorff-Larsen, D. L. Mobley, O. Ollila, C. Oostenbrink, P. Robustelli, V. A. Voelz, M. E. Wall, D. C. Wych, and M. K. Gilson, "Structure-based experimental datasets for benchmarking of protein simulation force fields," arXiv preprint arXiv:2303.11056 (2023).

### Appendix A: Deriving the first and second derivatives of the BICePs score.

The BICePs score is defined as the negative logarithm of the Bayes factor, which is the quotient of two model evidences:

$$f(\varepsilon) = -\ln(Z(\varepsilon)/Z_0), \quad (\text{A1})$$

where the evidence for model with force field parameters  $\varepsilon$  is

$$Z(\varepsilon) = \int \int \exp(-u(\mathbf{X}, \sigma | D, \varepsilon)) d\mathbf{X} d\sigma \quad (\text{A2})$$

and  $Z_0$  is the model evidence for the reference distribution, which is set to be a uniform ensemble (see Figure 1) and so, does not depend on  $\varepsilon$ . The partial derivatives of the BICePs score,  $f(\varepsilon)$ , with respect to the model parameters  $\varepsilon_i$ , is:

$$\frac{\partial f(\varepsilon)}{\partial \varepsilon_i} = \frac{\partial}{\partial \varepsilon_i} \left[ -\ln \frac{Z(\varepsilon)}{Z_0} \right] = -\frac{1}{Z} \frac{\partial Z(\varepsilon)}{\partial \varepsilon_i}, \quad (\text{A3})$$

where

$$\frac{\partial Z}{\partial \varepsilon_i} = \int \int \left[ -\frac{\partial u}{\partial \varepsilon_i} \right] \exp(-u) d\mathbf{X} d\sigma \quad (\text{A4})$$

This allows us to express the derivative of the BICePs score with respect to the force field parameter  $\varepsilon_i$  as:

$$\frac{\partial f(\varepsilon)}{\partial \varepsilon_i} = \int \int \frac{1}{Z(\varepsilon)} \left[ \frac{\partial u}{\partial \varepsilon_i} \right] \exp(-u) d\mathbf{X} d\sigma \quad (\text{A5})$$

which is the difference of Boltzmann averaged values of  $\partial u / \partial \varepsilon_i$ . This can also be explained in terms of prior energies. BICePs uses  $\lambda$  to scale the prior energies, where the reference ensemble is given  $\lambda = 0$ . Therefore, the average energy of the reference ensemble is zero and

$$\frac{\partial f(\varepsilon)}{\partial \varepsilon_i} = \left\langle \frac{\partial u}{\partial \varepsilon_i} \right\rangle \quad (\text{A6})$$

The Hessian matrix and corresponding second partial derivatives of the BICePs score is required for computing uncertainties of the inferred parameters by the covariance matrix (see equation 20), and when using a trust-region methods for optimization (see methods like ‘trust-ncg’, ‘trust-exact’ in ‘scipy.optimize.minimize’). Trust-region methods can be more robust for noisy gradients; they may perform better with noisy objective functions because it does not rely solely on the gradient information to determine the search direction. Instead, it uses a combination of the gradient and second-order information with the local quadratic model to estimate the direction of steepest descent. The Hessian matrix contains elements of second-order partial derivatives with respect to each parameter and gives the curvature of the objective function.

$$\mathbf{H} = \begin{bmatrix} \frac{\partial^2 f}{\partial \epsilon_1^2} & \frac{\partial^2 f}{\partial \epsilon_1 \partial \epsilon_2} & \cdots & \frac{\partial^2 f}{\partial \epsilon_1 \partial \epsilon_n} \\ \frac{\partial^2 f}{\partial \epsilon_2 \partial \epsilon_1} & \frac{\partial^2 f}{\partial \epsilon_2^2} & \cdots & \frac{\partial^2 f}{\partial \epsilon_2 \partial \epsilon_n} \\ \vdots & \vdots & \ddots & \vdots \\ \frac{\partial^2 f}{\partial \epsilon_n \partial \epsilon_1} & \frac{\partial^2 f}{\partial \epsilon_n \partial \epsilon_2} & \cdots & \frac{\partial^2 f}{\partial \epsilon_n^2} \end{bmatrix} \quad (\text{A7})$$

The second-order partial derivative of the BICePs score for parameters  $i$  and  $j$ , where  $i \neq j$  is given as

$$\frac{\partial^2 f}{\partial \epsilon_i \partial \epsilon_j} = \left[ -\frac{1}{Z(\epsilon)} \frac{\partial^2 Z(\epsilon)}{\partial \epsilon_i \partial \epsilon_j} + \frac{1}{Z(\epsilon)^2} \left( \frac{\partial Z(\epsilon)}{\partial \epsilon_i} \right) \left( \frac{\partial Z(\epsilon)}{\partial \epsilon_j} \right) \right], \quad (\text{A8})$$

where

$$\begin{aligned} \frac{\partial^2 Z}{\partial \epsilon_i \partial \epsilon_j} &= \frac{\partial}{\partial \epsilon_j} \left[ \iint \left( -\frac{\partial u}{\partial \epsilon_i} \right) \exp(-u) dX d\sigma \right] \\ &= \iint \left[ \left( \frac{\partial u}{\partial \epsilon_i} \right) \left( \frac{\partial u}{\partial \epsilon_j} \right) - \frac{\partial^2 u}{\partial \epsilon_i \partial \epsilon_j} \right] \exp(-u) dX d\sigma \end{aligned} \quad (\text{A9})$$

Putting this altogether and solving for equation A8 gives

$$\begin{aligned} \frac{\partial^2 f(\epsilon)}{\partial \epsilon_i \partial \epsilon_j} &= - \iint \frac{1}{Z(\epsilon)} \left[ \left( \frac{\partial u}{\partial \epsilon_i} \right) \left( \frac{\partial u}{\partial \epsilon_j} \right) \right] \exp(-u) dX d\sigma \\ &+ \iint \frac{1}{Z(\epsilon)} \left[ \frac{\partial^2 u}{\partial \epsilon_i \partial \epsilon_j} \right] \exp(-u) dX d\sigma \\ &+ \iint \frac{1}{Z(\epsilon)^2} \left( \frac{\partial u}{\partial \epsilon_i} \right) \left( \frac{\partial u}{\partial \epsilon_j} \right) \exp(-2u) dX d\sigma \end{aligned} \quad (\text{A10})$$

which reduces to

$$\begin{aligned} \frac{\partial^2 f(\epsilon)}{\partial \epsilon_i \partial \epsilon_j} &= \left\langle \frac{\partial^2 u}{\partial \epsilon_i \partial \epsilon_j} \right\rangle - \left( \left\langle \left( \frac{\partial u}{\partial \epsilon_i} \right) \left( \frac{\partial u}{\partial \epsilon_j} \right) \right\rangle \right. \\ &\quad \left. - \left\langle \left( \frac{\partial u}{\partial \epsilon_i} \right) \left( \frac{\partial u}{\partial \epsilon_j} \right) \right\rangle' \right), \end{aligned} \quad (\text{A11})$$

where the notation  $\langle \cdot \rangle'$  denotes the average with respect to  $(\frac{1}{Z} \exp(-u))^2$ . When  $i = j$  (diagonal elements of the Hessian), the second-order partial derivatives of the BICePs score

can be seen as the difference of the Boltzmann-averaged second-order partial derivative of the energy and the variance in its first-order partial derivative:

$$\frac{\partial^2 f(\epsilon)}{\partial \epsilon^2} = \left\langle \frac{\partial^2 u}{\partial \epsilon^2} \right\rangle - \left( \left\langle \left( \frac{\partial u}{\partial \epsilon} \right)^2 \right\rangle - \left\langle \frac{\partial u}{\partial \epsilon} \right\rangle^2 \right) \quad (\text{A12})$$

To compute the derivatives of the BICePs score, we need the first and second derivatives of the BICePs energy function  $u$ , which consists of taking derivatives of the negative logarithm of the posterior, since  $u = -\log p(X, \sigma | D, \epsilon)$ . The derivative of this function with respect to some force field parameter  $\epsilon$  is

$$\begin{aligned} \frac{\partial u}{\partial \epsilon_i} &= \frac{\partial E}{\partial \epsilon_i} \left( \sum_{r=1}^N -\log \left[ \frac{\exp(-E(X_r | \epsilon))}{\sum_X \exp(-E(X | \epsilon))} \right] \right) \\ &= - \sum_{r=1}^N \frac{\sum_X \exp(-E(X | \epsilon))}{\exp(-E(X | \epsilon))} \frac{\partial}{\partial \epsilon_i} \left[ -\frac{\frac{\partial E(X | \epsilon)}{\partial \epsilon_i} \exp(-E(X | \epsilon))}{\sum_X \exp(-E(X | \epsilon))} \right. \\ &\quad \left. - \frac{\sum_X -\exp(-E(X | \epsilon)) \frac{\partial E(X | \epsilon)}{\partial \epsilon_i} \exp(-E(X | \epsilon))}{(\sum_X \exp(-E(X | \epsilon)))^2} \right] \\ &= \sum_{r=1}^N \left\{ \frac{\partial E(X_r | \epsilon)}{\partial \epsilon_i} - \frac{\sum_X \exp(-E(X | \epsilon)) \frac{\partial E(X | \epsilon)}{\partial \epsilon_i}}{\sum_X \exp(-E(X | \epsilon))} \right\} \\ &= \sum_{r=1}^N \left\{ \frac{\partial E(X_r | \epsilon)}{\partial \epsilon_i} - \left\langle \frac{\partial E(X | \epsilon)}{\partial \epsilon_i} \right\rangle \right\} \end{aligned} \quad (\text{A13})$$

The second derivative is

$$\begin{aligned} \frac{\partial^2 u}{\partial \epsilon_i \partial \epsilon_j} &= \sum_{r=1}^N \left[ \frac{\partial^2 E(X_r | \epsilon)}{\partial \epsilon_i \partial \epsilon_j} - \frac{\sum_X \exp(-E(X | \epsilon)) \frac{\partial^2 E(\mathbf{X} | \epsilon)}{\partial \epsilon_i \partial \epsilon_j}}{\sum_X \exp(-E(X | \epsilon))} \right. \\ &\quad + \frac{\sum_X \exp(-E(X | \epsilon)) \left( \frac{\partial E(\mathbf{X} | \epsilon)}{\partial \epsilon_i} \right) \left( \frac{\partial E(\mathbf{X} | \epsilon)}{\partial \epsilon_j} \right)}{\sum_X \exp(-E(X | \epsilon))} \\ &\quad \left. - \frac{\sum_X \exp(-2E(X | \epsilon)) \left( \frac{\partial E(\mathbf{X} | \epsilon)}{\partial \epsilon_i} \right) \left( \frac{\partial E(\mathbf{X} | \epsilon)}{\partial \epsilon_j} \right)}{(\sum_X \exp(-E(X | \epsilon)))^2} \right] \end{aligned} \quad (\text{A14})$$

which can be reduced to

$$\begin{aligned} \frac{\partial^2 u}{\partial \epsilon_i \partial \epsilon_j} &= \sum_{r=1}^N \left\{ \frac{\partial^2 E(X_r | \epsilon)}{\partial \epsilon_i \partial \epsilon_j} - \left\langle \frac{\partial^2 E(\mathbf{X} | \epsilon)}{\partial \epsilon_i \partial \epsilon_j} \right\rangle \right. \\ &\quad + \left\langle \left( \frac{\partial E(\mathbf{X} | \epsilon)}{\partial \epsilon_i} \right) \left( \frac{\partial E(\mathbf{X} | \epsilon)}{\partial \epsilon_j} \right) \right\rangle \\ &\quad \left. - \frac{\sum_X \exp(-2E(X | \epsilon)) \left( \frac{\partial E(\mathbf{X} | \epsilon)}{\partial \epsilon_i} \right) \left( \frac{\partial E(\mathbf{X} | \epsilon)}{\partial \epsilon_j} \right)}{(\sum_X \exp(-E(X | \epsilon)))^2} \right\} \end{aligned} \quad (\text{A15})$$

and when  $i = j$ , the second-order partial derivative of the en-

ergy function becomes

$$\frac{\partial^2 u}{\partial \varepsilon^2} = \sum_{r=1}^N \left\{ \frac{\partial^2 E(X_r | \varepsilon)}{\partial \varepsilon^2} - \left\langle \frac{\partial^2 E(X | \varepsilon)}{\partial \varepsilon^2} \right\rangle + \left\langle \left( \frac{\partial E(X | \varepsilon)}{\partial \varepsilon} \right)^2 \right\rangle - \left\langle \frac{\partial E(X | \varepsilon)}{\partial \varepsilon} \right\rangle^2 \right\} \quad (\text{A16})$$

### Appendix B: Kofinger & Hummer's toy polymer model

As mentioned in the main text, the two dimensional polymer model<sup>3</sup> consists of a string of  $n = 100$  beads separated by a unit of length, where  $\Delta\phi_i$  is the angle between the two bond vectors  $v_i$  and  $v_{i+1}$ . The associated probability of a polymer with  $n$  beads is given by

$$\begin{aligned} p(\Delta\phi | \mu, \kappa) &= \prod_{i=1}^{n-1} p(\Delta\phi_i | \mu_i, \kappa_i) \\ &= \prod_{i=1}^{n-1} \frac{\exp(\kappa_i \cos(\Delta\phi_i - \mu_i))}{2\pi I_0(\kappa_i)} \end{aligned} \quad (\text{B1})$$

where  $I_0(\kappa)$  is the modified Bessel function of order zero and  $\mu_i$  introduces directional biases. The parameters  $\kappa_i > 0$  determine the stiffness of the polymer at positions  $i$ . Prior energy,  $E$  of the polymer configuration follow the Boltzmann distribution, which corresponds to

$$E = -\log \prod_{i=1}^{n-1} p(\Delta\phi_i | \mu_i, \kappa_i) \quad (\text{B2})$$

The authors did not provide derivatives of the toy model energy function, so we will briefly derive derivatives of the prior energies that will be used in our algorithm. The first derivative of the prior energy  $E$  with respect to  $\kappa$  is

$$\begin{aligned} \frac{\partial E}{\partial \kappa} &= -\sum_{i=1}^{n-1} \frac{\partial}{\partial \kappa} \log p(\Delta\phi_i | \mu_i, \kappa_i) \\ &= -\sum_{i=1}^{n-1} \frac{1}{p(\Delta\phi_i | \mu_i, \kappa_i)} \frac{\partial p(\Delta\phi_i | \mu_i, \kappa_i)}{\partial \kappa}, \end{aligned} \quad (\text{B3})$$

where the derivative of the von Mises distribution with respect to  $\kappa$  is

$$\begin{aligned} \frac{\partial p}{\partial \kappa} &= \frac{\exp(\kappa_i \cos(\mu_i - \Delta\phi_i)) \cos(\mu_i - \Delta\phi_i)}{2\pi I_0(\kappa_i)} \\ &\quad - \frac{\exp(\kappa_i \cos(\mu_i - \Delta\phi_i)) I_1(\kappa_i)}{2\pi I_0^2(\kappa_i)} \end{aligned} \quad (\text{B4})$$

which is relatively straightforward since the derivative of the modified Bessel function merely increases it's order. Next, the second derivative of  $E$  with respect to  $\kappa_i$ :

$$\frac{\partial^2 E}{\partial \kappa_i^2} = \sum \left\{ -\frac{1}{p} \frac{\partial^2 p}{\partial \kappa_i^2} + \left( \frac{1}{p} \frac{\partial p}{\partial \kappa_i} \right)^2 \right\}, \quad (\text{B5})$$

where the second derivative of the von Mises distribution w.r.t  $\kappa_i$  is

$$\begin{aligned} \frac{\partial^2 p}{\partial \kappa_i^2} &= \left[ \frac{\exp(\kappa_i \cos(\mu_i - \Delta\phi_i)) \left( \frac{I_0(\kappa_i)}{2} + \frac{I_2(\kappa_i)}{2} \right)}{2\pi I_0^2(\kappa_i)} \right. \\ &\quad + \frac{\exp(\kappa_i \cos(\mu_i - \Delta\phi_i)) \cos^2(\mu_i - \Delta\phi_i)}{2\pi I_0(\kappa_i)} \\ &\quad - \frac{\exp(\kappa_i \cos(\mu_i - \Delta\phi_i)) \cos(\mu_i - \Delta\phi_i) I_1(\kappa_i)}{\pi I_0^2(\kappa_i)} \\ &\quad \left. + \frac{\exp(\kappa_i \cos(\mu_i - \Delta\phi_i)) I_1^2(\kappa_i)}{\pi I_0^3(\kappa_i)} \right] \end{aligned} \quad (\text{B6})$$

**Appendix C: Supplemental Information**

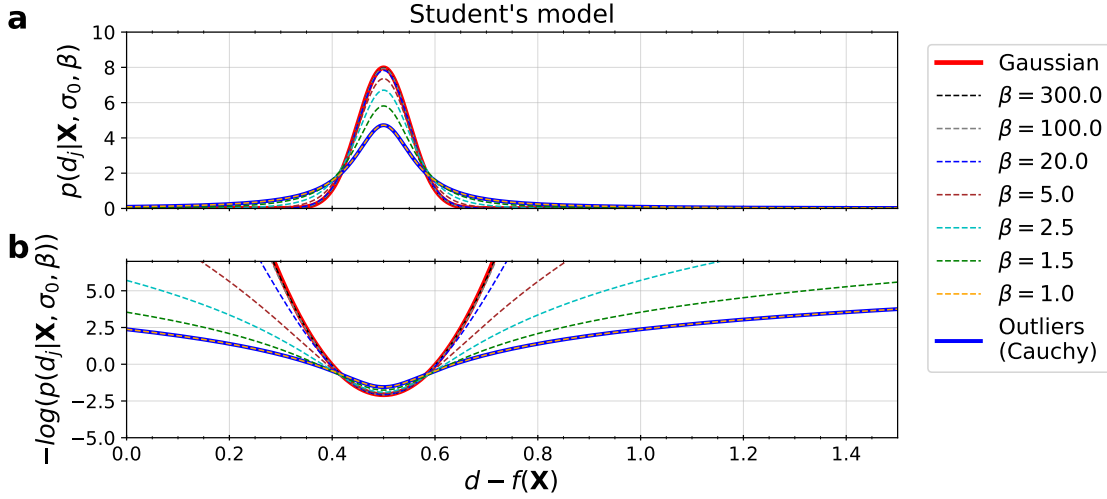


Figure S1. The probability density function (a) and energy landscape (b) of the marginal likelihood for the Student’s model with respect to the replica-averaged forward model data  $f(\mathbf{X})$ . The colored curves are different values of nuisance parameter  $\beta$ . The Student’s model is equivalent to the Outliers model (Cauchy) when  $\beta = 1$ , and as  $\beta$  goes to infinity, the pdf becomes Gaussian and the energy becomes harmonic.

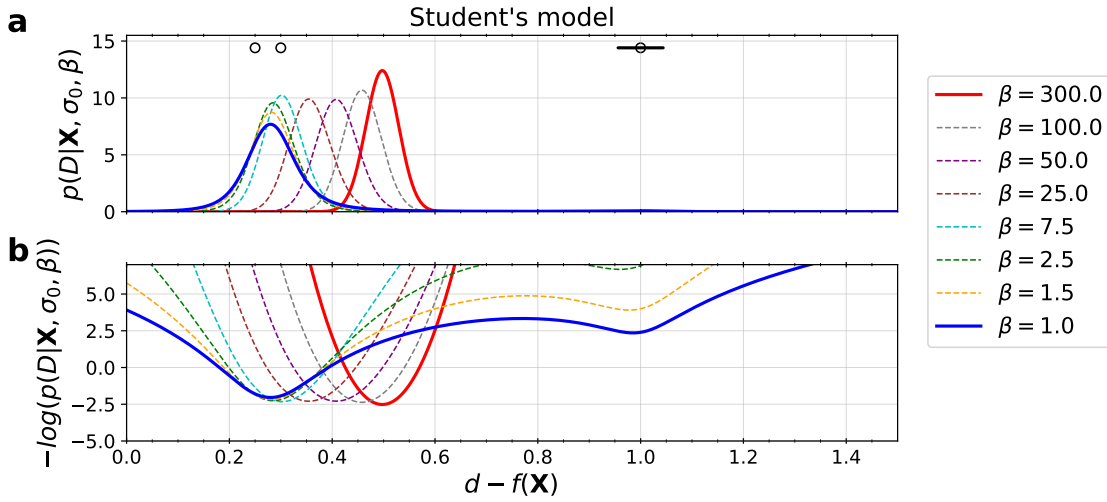


Figure S2. The probability density function (a) computed as  $p(D|\mathbf{X}, \sigma_0, \beta) = \prod_j^{N_j} p(d_j|\mathbf{X}, \sigma_0, \beta)$  and energy landscape (b) of the marginal likelihood for the Student’s model with respect to the replica-averaged forward model data  $f(\mathbf{X})$  using multiple data points. Shown here, are three data points, two good data points  $\{0.25, 0.3\}$  and one outlier  $\{1.0\}$ . The Cauchy likelihood ( $\beta = 1$ ) is centered about the mean of the two good data points, demonstrating that this model can distinguish the good and bad data. The standard Gaussian likelihood ( $\beta = 300$ ) is centered about the mean of all three data points. The colored curves are different values of nuisance parameter  $\beta$ .

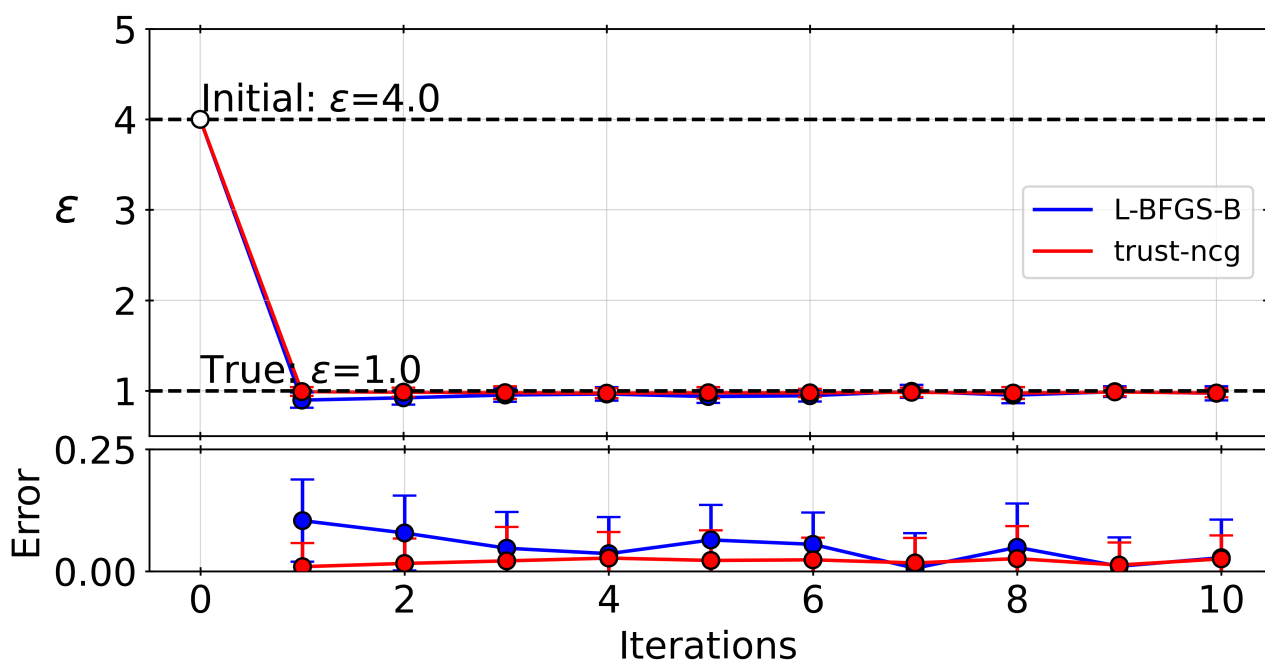


Figure S3. Trust-region optimization with BICePs is found to converge faster and be more robust than L-BFGS-B. Here, we compare first-order L-BFGS-B method (blue) to the second-order Trust-NCG optimization method (red). A total of 25 independent rounds of parameter ( $\epsilon$ ) optimizations using the BICePs score for a maximum of ten iterations. Data points are placed at the mean value for each iteration and error bars are the standard deviation. It is typical that the trust-ncg method reaches convergence slightly faster (the 4th iteration), and the L-BFGS-B method tends to slightly overshoot the "True"  $\epsilon$  value on the first iteration.

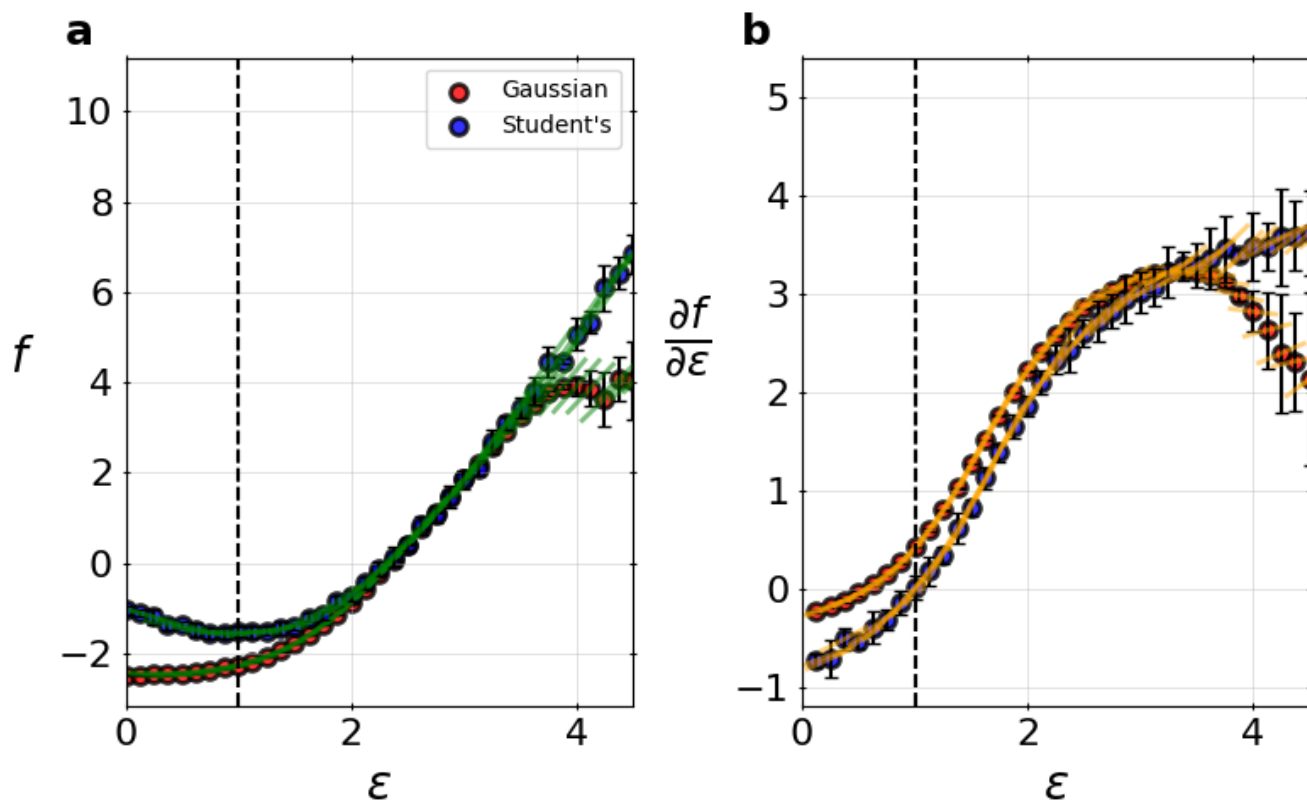


Figure S4. **The BICePs score landscape using a standard Gaussian likelihood versus a Student's likelihood in the presence of systematic error.** (a) 1-D scans over  $\epsilon$  to reveal the landscape of the BICePs score (scatter dots). The green tangent lines are the derivatives at each  $\epsilon$  value. Uncertainties in the BICePs scores and derivatives come from five independent scans along  $\epsilon$ . (b) The derivative of the BICePs score (scatter dots) and the second derivative of the BICePs score (yellow lines) at each epsilon value. The dotted black line at  $\epsilon^* = 1.0$  shows the true value, which is where the derivative of the BICePs score equals zero. BICePs calculations are run using the Student's model for 100k steps with 8 replicas. Systematic error ( $+4\text{\AA}$  shift) was induced to the 2-11 distance, with a total experimental error of  $\sigma_{data} = 1.41$ .

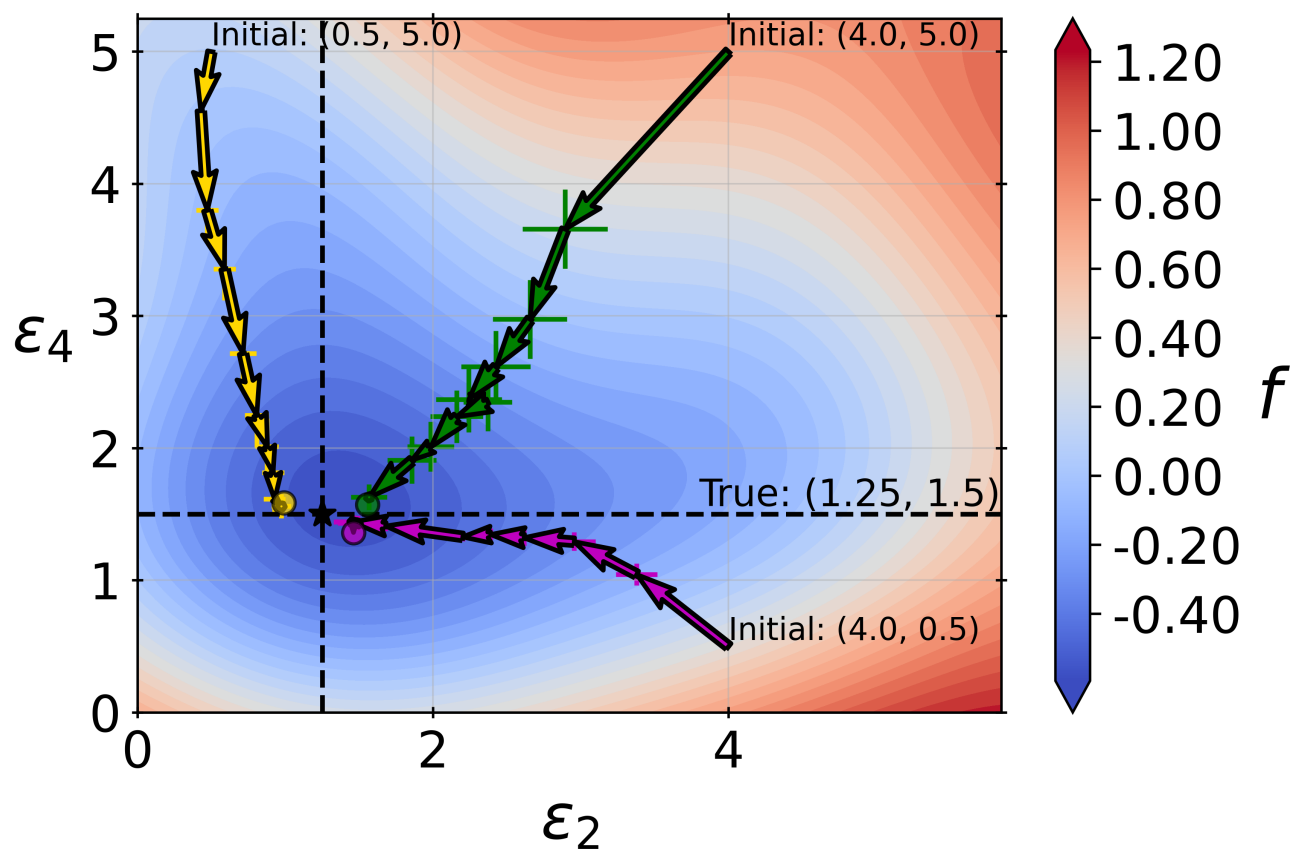


Figure S5. Average traces over a total of 25 independent rounds of parameter  $(\epsilon_2, \epsilon_4)$  optimizations using first-order optimization method (L-BFGS-B) with BICePs, for a maximum of ten iterations. Traces are unable to fully reach the "True" iteration strength parameters  $(\epsilon_2^* = 1.25, \epsilon_4^* = 1.5)$  within 10 iterations when starting from different initial parameters  $(\epsilon_2^0, \epsilon_4^0) = \{(0.5, 5.0), (4.0, 5.0), (4.0, 0.5)\}$ . The BICePs score landscape was generated from the average values of five scans over  $\epsilon_2$  and  $\epsilon_4$ . All calculations used the Student's model with 200k MCMC steps and 8 replicas.

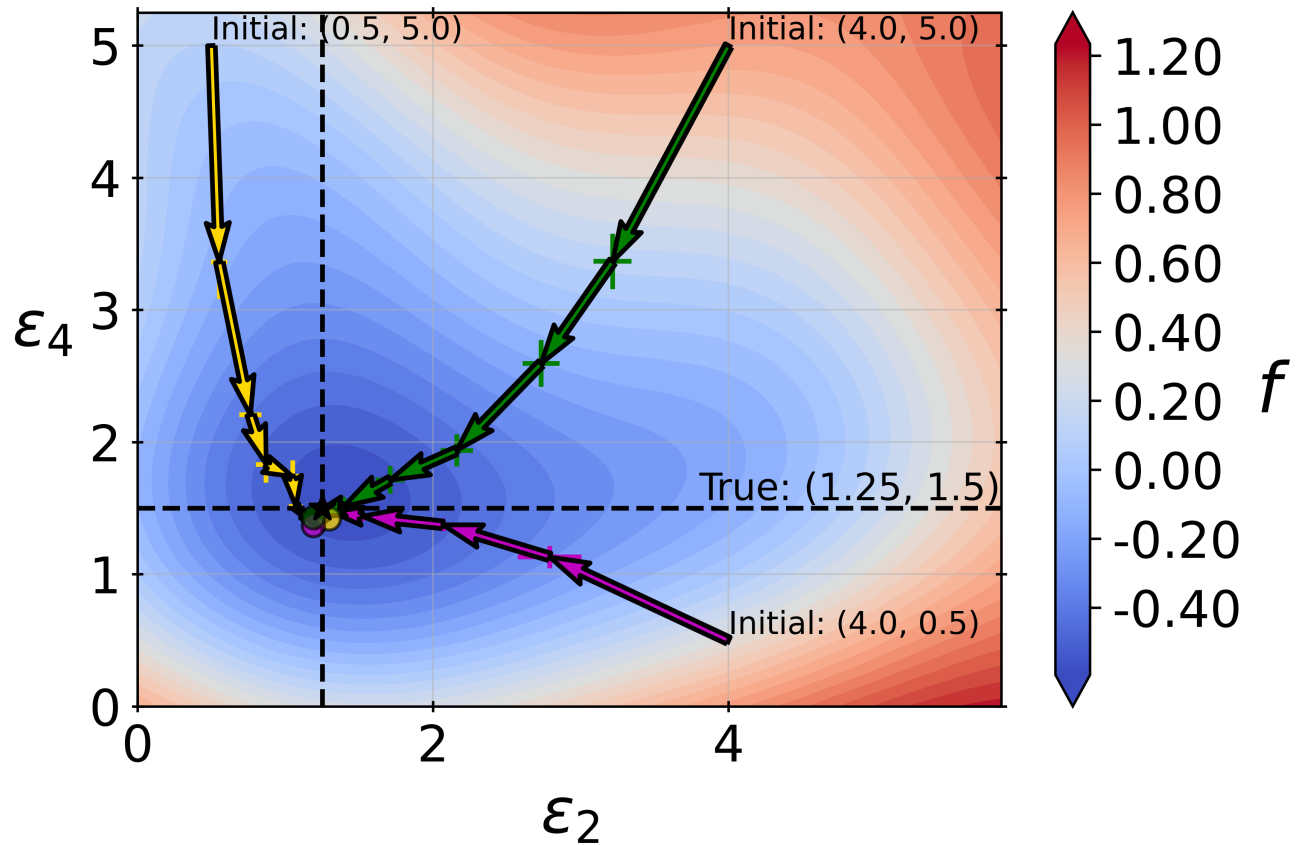


Figure S6. Average traces over a total of 25 independent rounds of parameter  $(\epsilon_2, \epsilon_4)$  optimizations using second-order (trust-ncg) method with BICePs, for a maximum of ten iterations. Optimizations converge to the "True" optimal iteration strength parameters  $(\epsilon_2^* = 1.25, \epsilon_4^* = 1.5)$  when starting from different initial parameters  $(\epsilon_2^0, \epsilon_4^0) = \{(0.5, 5.0), (4.0, 5.0), (4.0, 0.5)\}$ . The BICePs score landscape was generated from the average values of five scans over  $\epsilon_2$  and  $\epsilon_4$ . All calculations used the Student's model with 200k MCMC steps and 8 replicas.

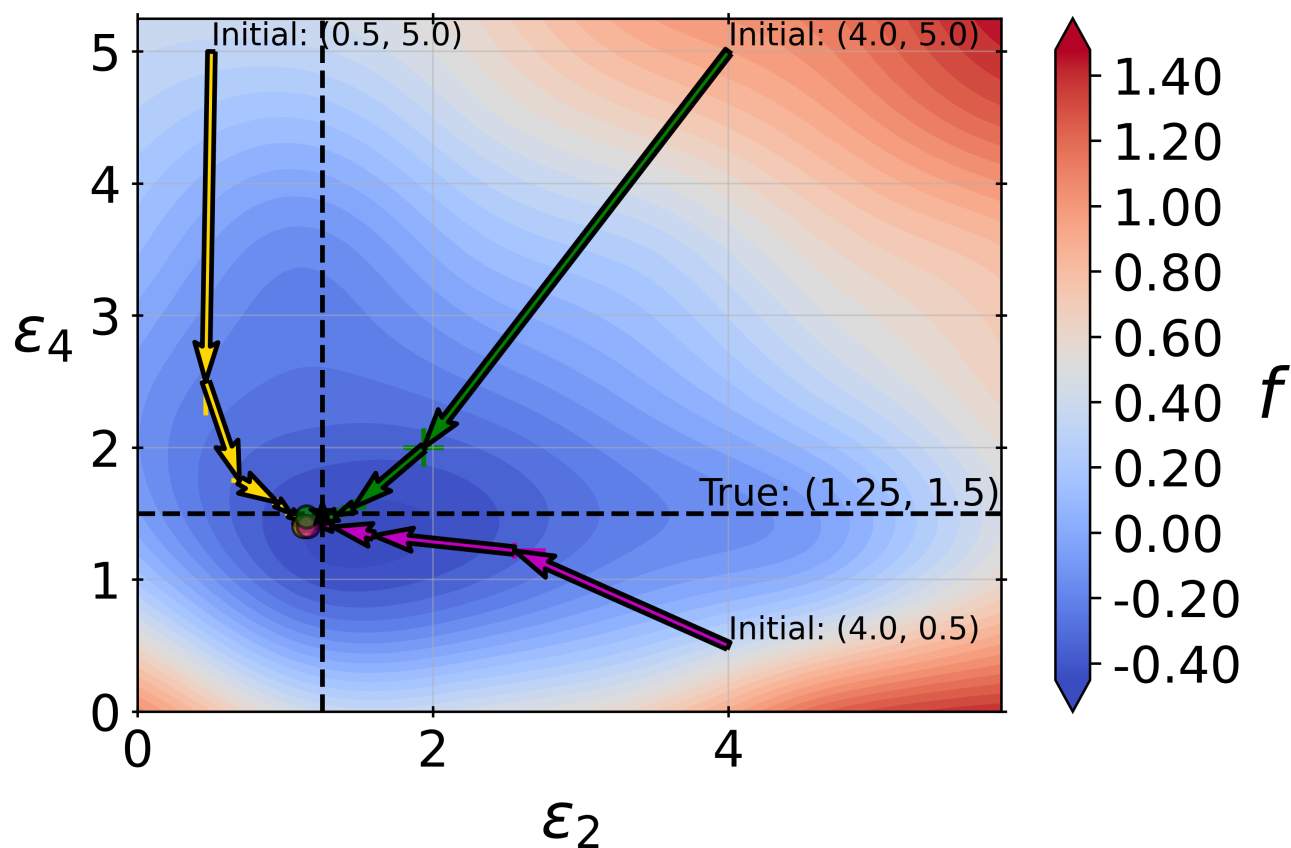


Figure S7. Average traces over a total of 25 independent rounds of parameter  $(\epsilon_2, \epsilon_4)$  optimizations using second-order (trust-ncg) method with BICePs, for a maximum of ten iterations. In these tests, no error was added to the experimental data. Optimizations converge to the "True" parameters  $(\epsilon_2^* = 1.25, \epsilon_4^* = 1.5)$  when starting from different initial parameters  $(\epsilon_2^0, \epsilon_4^0) = \{(0.5, 5.0), (4.0, 5.0), (4.0, 0.5)\}$ . The BICePs score landscape was generated from the average values of five scans over  $\epsilon_2$  and  $\epsilon_4$ . All calculations used the Student's model with 200k MCMC steps and 32 replicas. Average optimized parameter values were  $(\epsilon_2 = 1.12 \pm 0.39, \text{ and } \epsilon_4 = 1.43 \pm 0.34)$ , where the uncertainties are estimated from inverse Hessian.

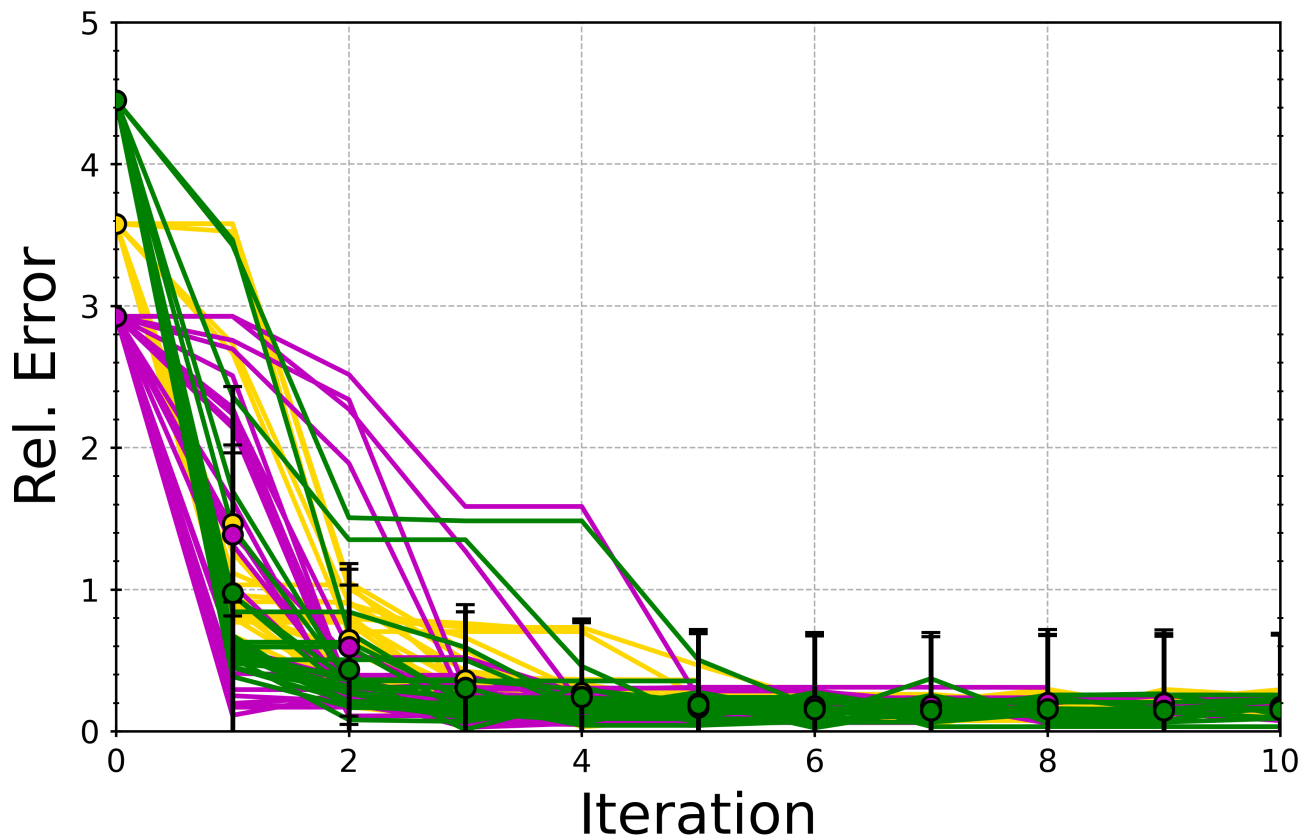


Figure S8. Accuracy profiles for  $(\epsilon_2, \epsilon_4)$  optimizations using second-order (trust-ncg) method with BICePs, for a total of 25 independent rounds and a maximum of ten iterations. In these tests, no error was added to the experimental data. Optimizations converge to the "True" parameters  $(\epsilon_2^* = 1.25, \epsilon_4^* = 1.5)$  with a relative error less than 1.0 when starting from different initial parameters  $(\epsilon_2^0, \epsilon_4^0) = \{(0.5, 5.0), (4.0, 5.0), (4.0, 0.5)\}$ . All calculations used the Student's model with 200k MCMC steps and 32 replicas. Average optimized parameter values were  $(\epsilon_2 = 1.12 \pm 0.39, \text{ and } \epsilon_4 = 1.43 \pm 0.34)$ , where the uncertainties are estimated from inverse Hessian. Error bars represent uncertainties estimated from the inverse Hessian, averaged over the 25 independent optimizations.

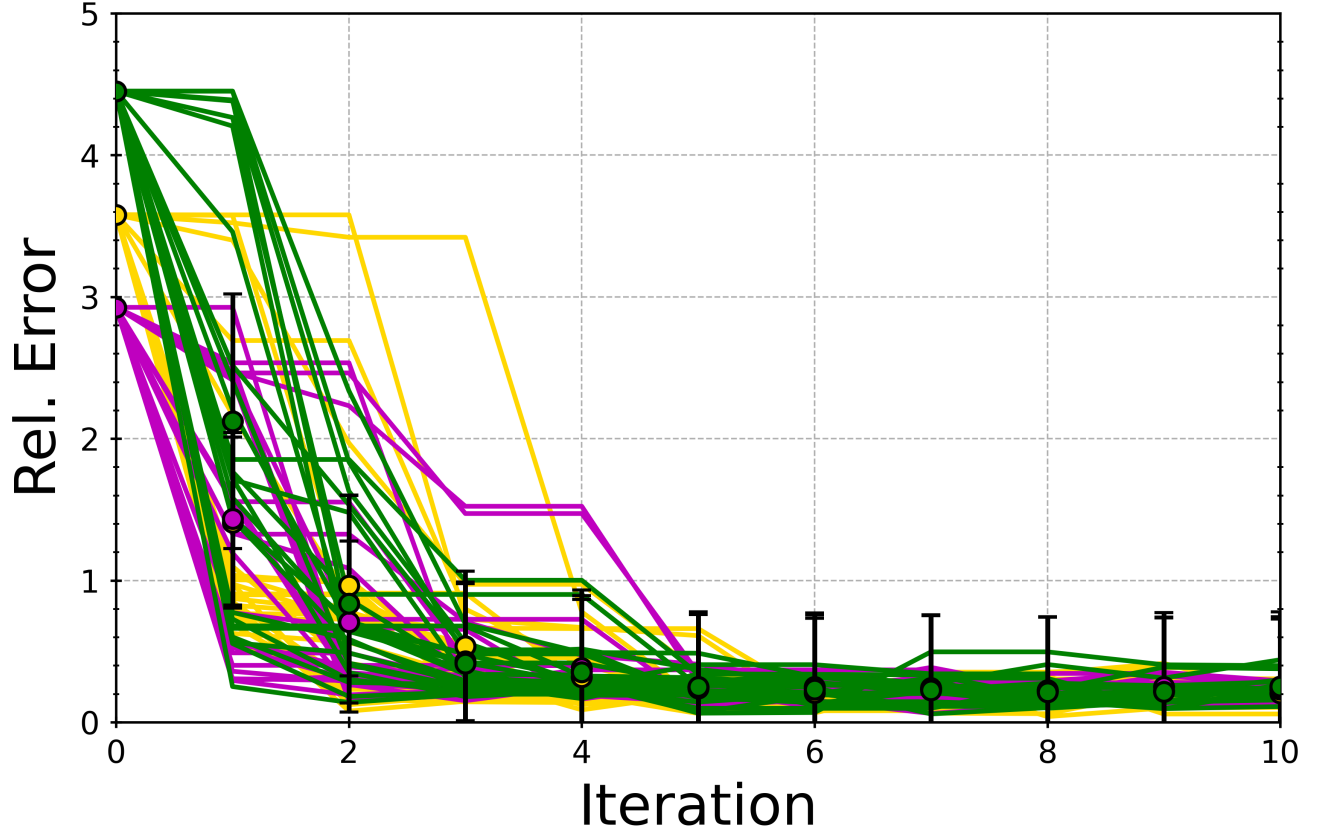


Figure S9. Accuracy profiles for  $(\epsilon_2, \epsilon_4)$  optimizations using second-order (trust-ncg) method with BICePs, for a total of 25 independent rounds and a maximum of ten iterations. In these tests, the experimental data was corrupted with systematic error in the 2–11 and 4–9 distances for +3 and +3.5Å shift, respectively. The total error in the data is  $\sigma_{data} = 1.63$ . Optimizations converge to the "True" optimal iteration strength parameters ( $\epsilon_2^* = 1.25$ ,  $\epsilon_4^* = 1.5$ ) with a relative error less than 1.0 when starting from different initial parameters  $(\epsilon_2^0, \epsilon_4^0) = \{(0.5, 5.0), (4.0, 5.0), (4.0, 0.5)\}$ . Error bars represent uncertainties estimated from the inverse Hessian, averaged over the 25 independent optimizations. All calculations used the Student's model with 200k MCMC steps and 32 replicas.

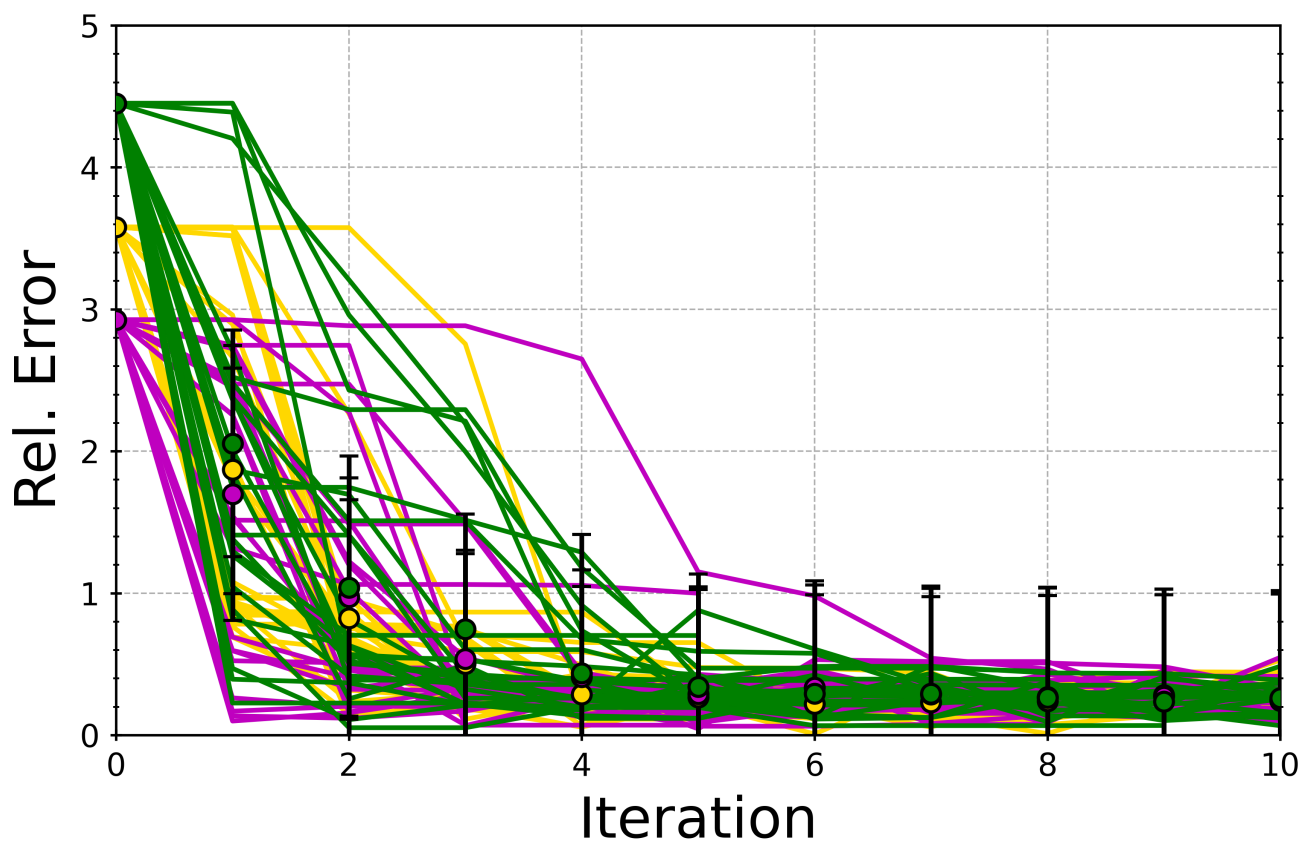


Figure S10. Accuracy profiles for  $(\epsilon_2, \epsilon_4)$  optimizations using a second-order (trust-ncg) method with BICePs, for a total of 25 independent rounds and a maximum of ten iterations. In these tests, the experimental data was corrupted with systematic error in the 2–11 and 4–9 distances for +3 and +3.5 Å shift, respectively. The total error in the data is  $\sigma_{data} = 1.63$ . Optimizations converge to the "True" parameters  $(\epsilon_2^* = 1.25, \epsilon_4^* = 1.5)$  with a relative error less than 1.0 when starting from different initial parameters  $(\epsilon_2^0, \epsilon_4^0) = \{(0.5, 5.0), (4.0, 5.0), (4.0, 0.5)\}$ . Error bars represent uncertainties estimated from the inverse Hessian, averaged over the 25 independent optimizations. For the optimization traces that remain unconverged for 10 iterations, the relative error was determined to be  $0.24 \pm 0.75$ , where the uncertainty is estimated from the inverse Hessian. All calculations used the Student's model with 200k MCMC steps and 16 replicas.

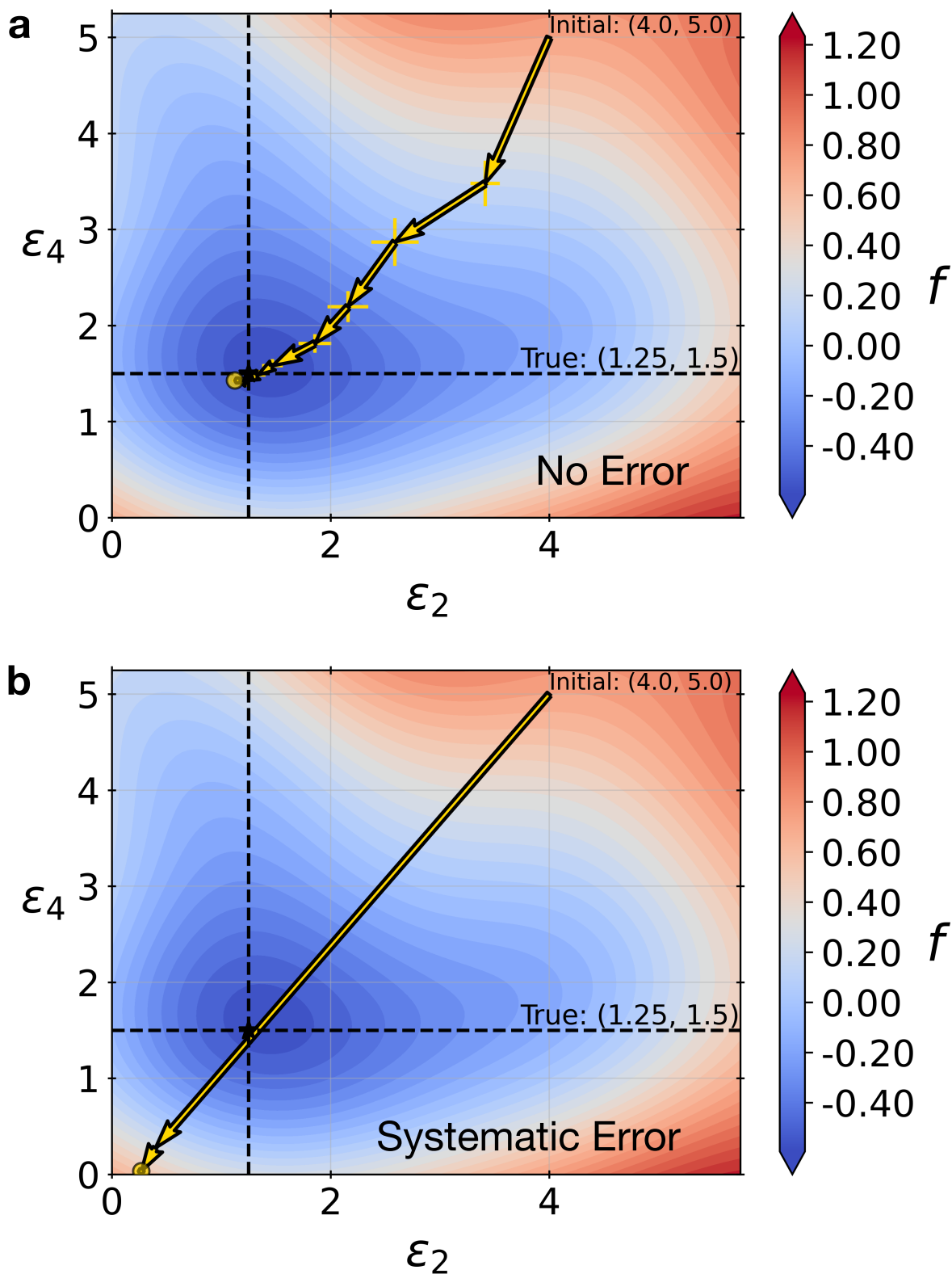


Figure S11. The accuracy of a standard Gaussian likelihood drops in the presence of systematic error. Demonstrating optimization accuracy when the data is corrupted with and without systematic error using  $\epsilon_2 = 4.0$  and  $\epsilon_4 = 5.0$  as initial parameters, same conditions as in Figure 5, where the "True" parameters are ( $\epsilon_2^* = 1.25, \epsilon_4^* = 1.5$ ). (a) The Gaussian likelihood performs great when using experimental data not affected by systematic error. (b) The accuracy suffers when the data is corrupted with systematic error in the 2-11 and 4-9 distances for +3 and +3.5Å shift, respectively. The total error in the data is  $\sigma_{data} = 1.63$ . All results shown here are averages over 25 independent optimizations, and error bars are computed as standard error of the mean for each iteration.

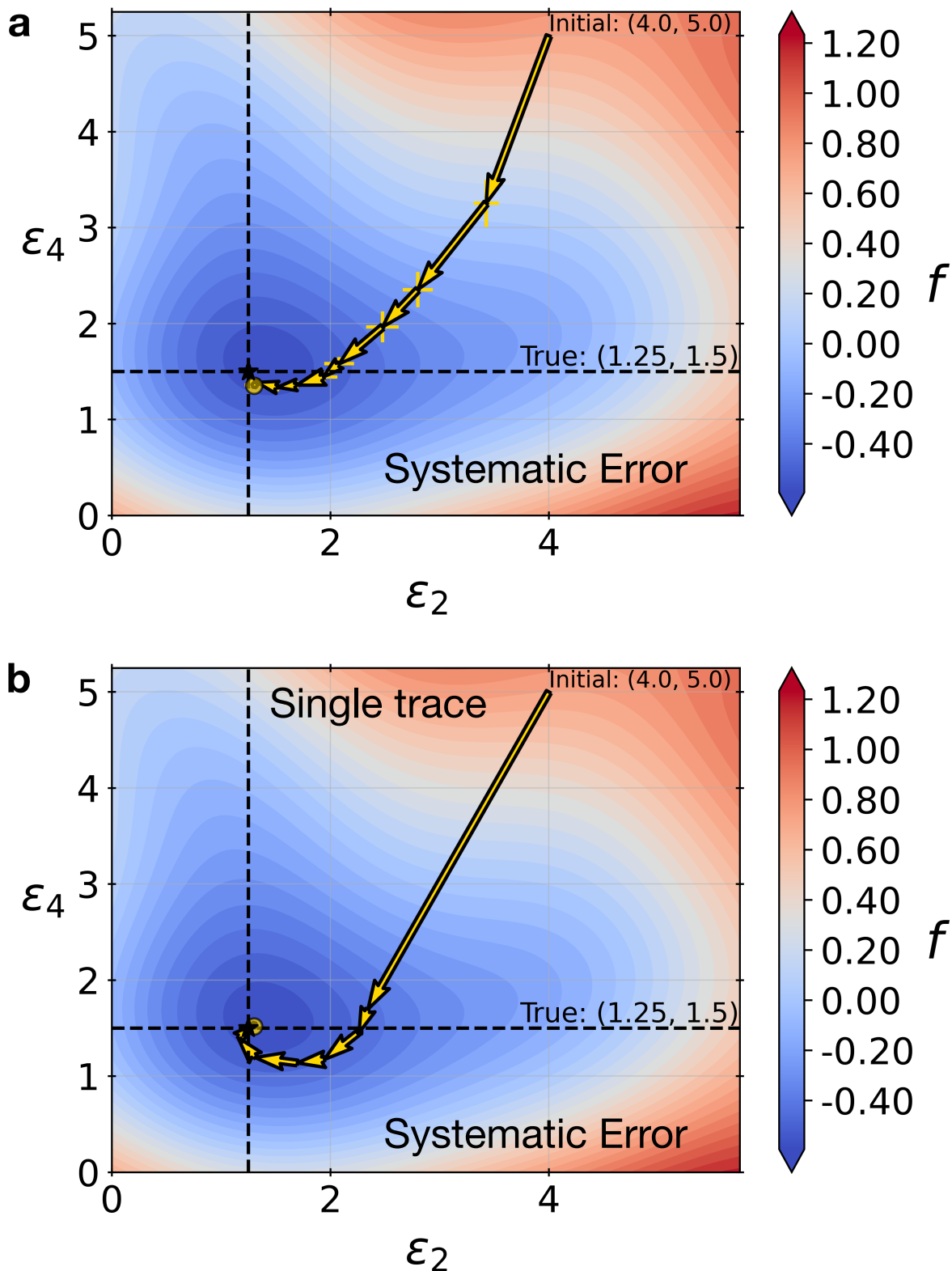


Figure S12. The accuracy of the Student's model is very robust in the presence of systematic error. (a) Average traces over 25 independent optimizations when the data is corrupted with systematic error in the 2–11 and 4–9 distances for +3 and +3.5Å shift, respectively. The total error in the data is  $\sigma_{data} = 1.63$ . (b) A single representative trace demonstrating convergence to the "True" parameters ( $\epsilon_2^* = 1.25, \epsilon_4^* = 1.5$ )

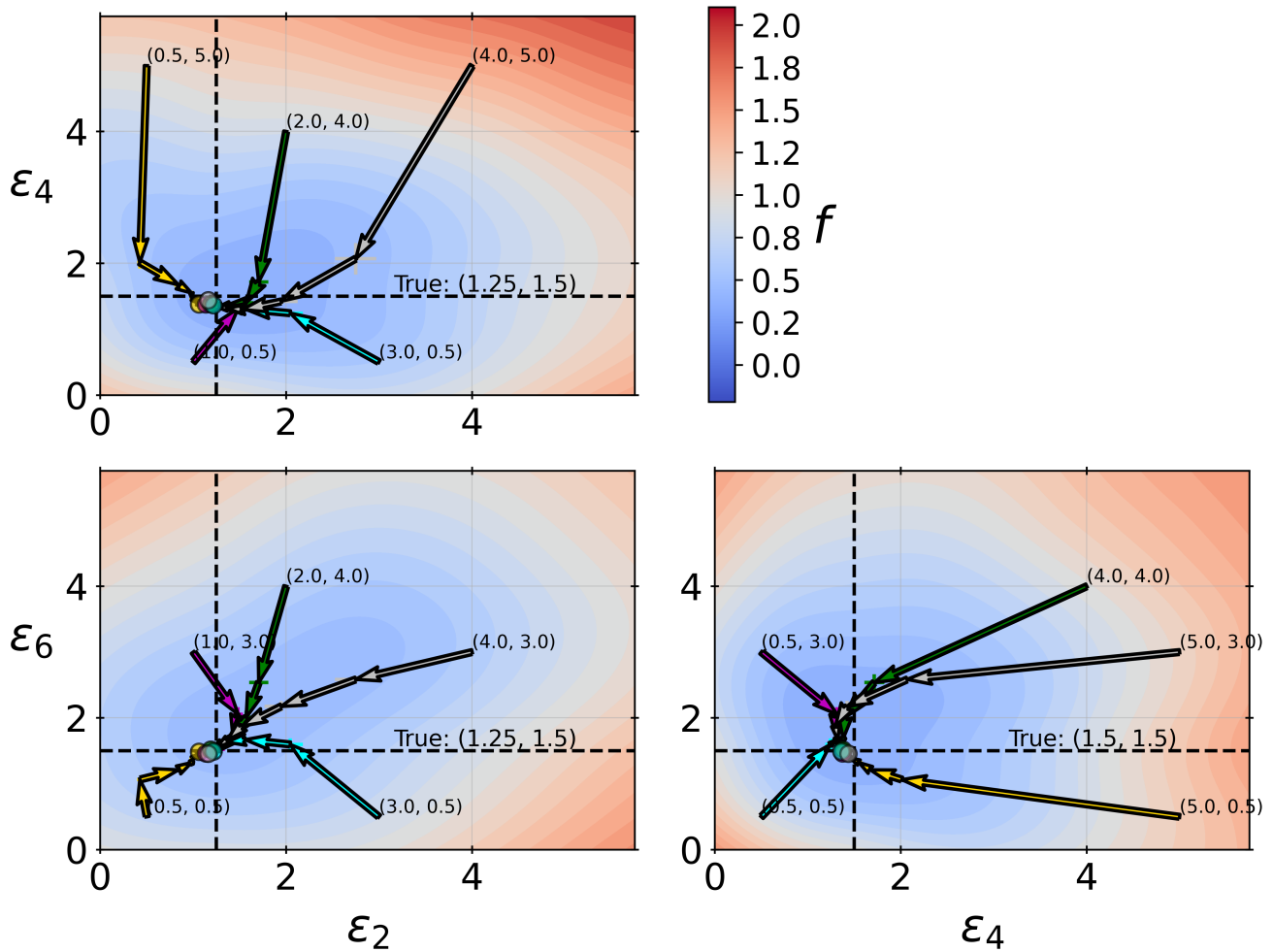


Figure S13. Average traces over a total of 25 independent rounds of parameter  $(\epsilon_2, \epsilon_4, \epsilon_6)$  optimizations using second-order (trust-ncg) method with BICePs, for a maximum of ten iterations. Optimizations converge to the "True" optimal iteration strength parameters ( $\epsilon_2^* = 1.25$ ,  $\epsilon_4^* = 1.5$ ,  $\epsilon_6^* = 1.5$ ) when starting from different initial parameters. All calculations used the Student's model with 200k MCMC steps and 32 replicas.

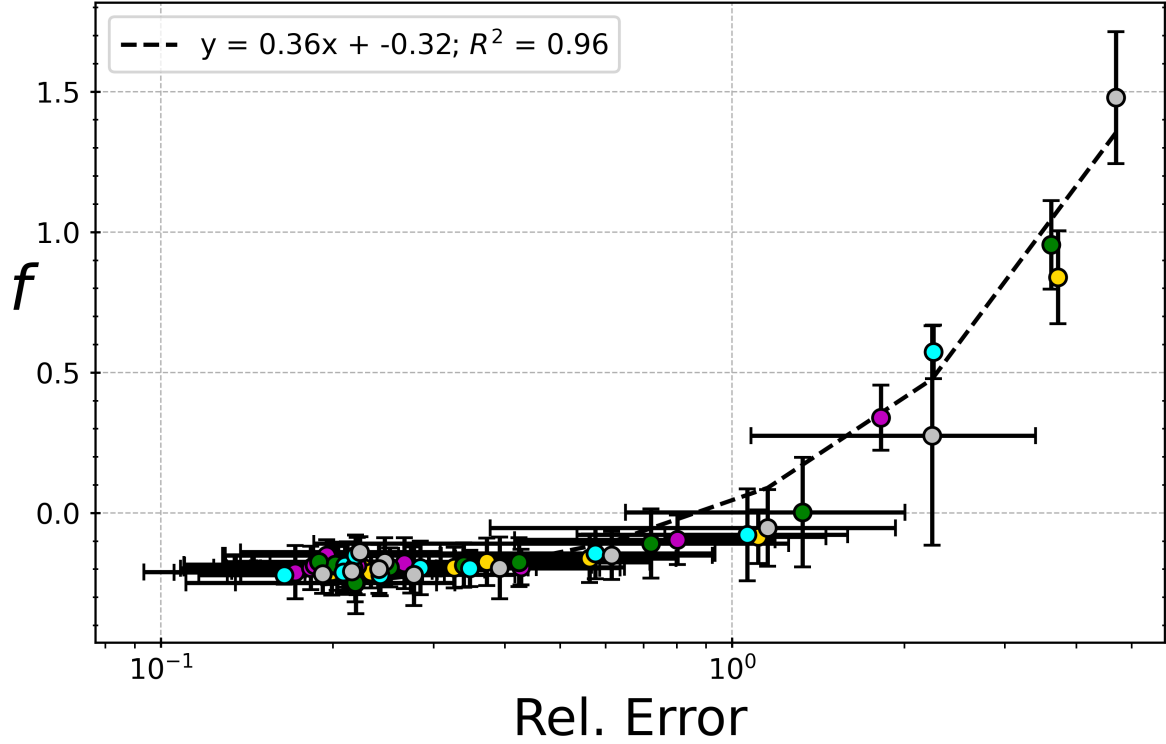


Figure S14. Sensitivity analysis of parameter  $(\epsilon_2, \epsilon_4, \epsilon_6)$  optimizations from various initial conditions. Regardless of different starting parameters, optimizations universally converge to "True" optimal iteration strength parameters  $(\epsilon_2^* = 1.25, \epsilon_4^* = 1.5, \epsilon_6^* = 1.5)$  and succeed in diminishing the relative error. All BICePs score optimizations used 32 BICePs replicas with the Student's likelihood model, and 200k MCMC steps per iteration. The dashed line is a linear fitting with equation  $y = 0.36x - 0.32$ , resulting in a strong correlation between the BICePs score and relative model error ( $R^2 = 0.96$ ).

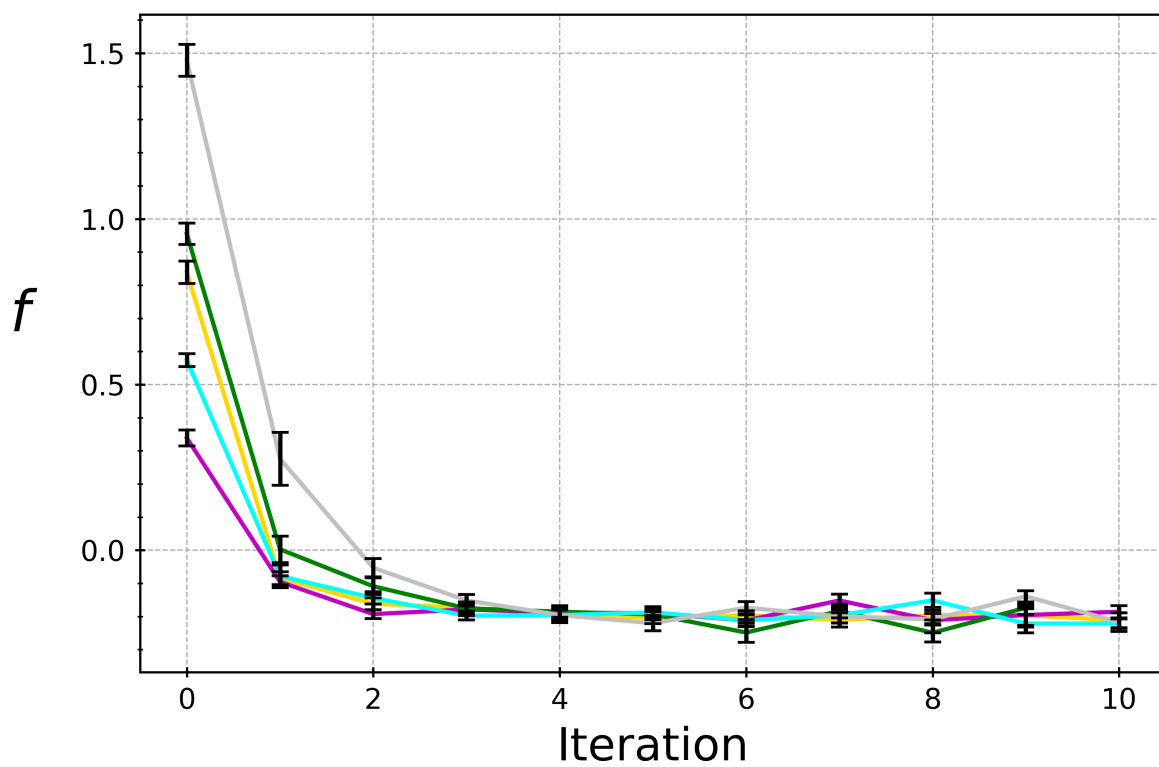


Figure S15. Minimization of the BICePs score,  $f$  is demonstrated when averaging over 25 independent rounds of parameter  $(\epsilon_2, \epsilon_4, \epsilon_6)$  optimizations using second-order (trust-ncg) method, for a maximum of ten iterations. Error bars represent the standard error over the 25 optimizations.

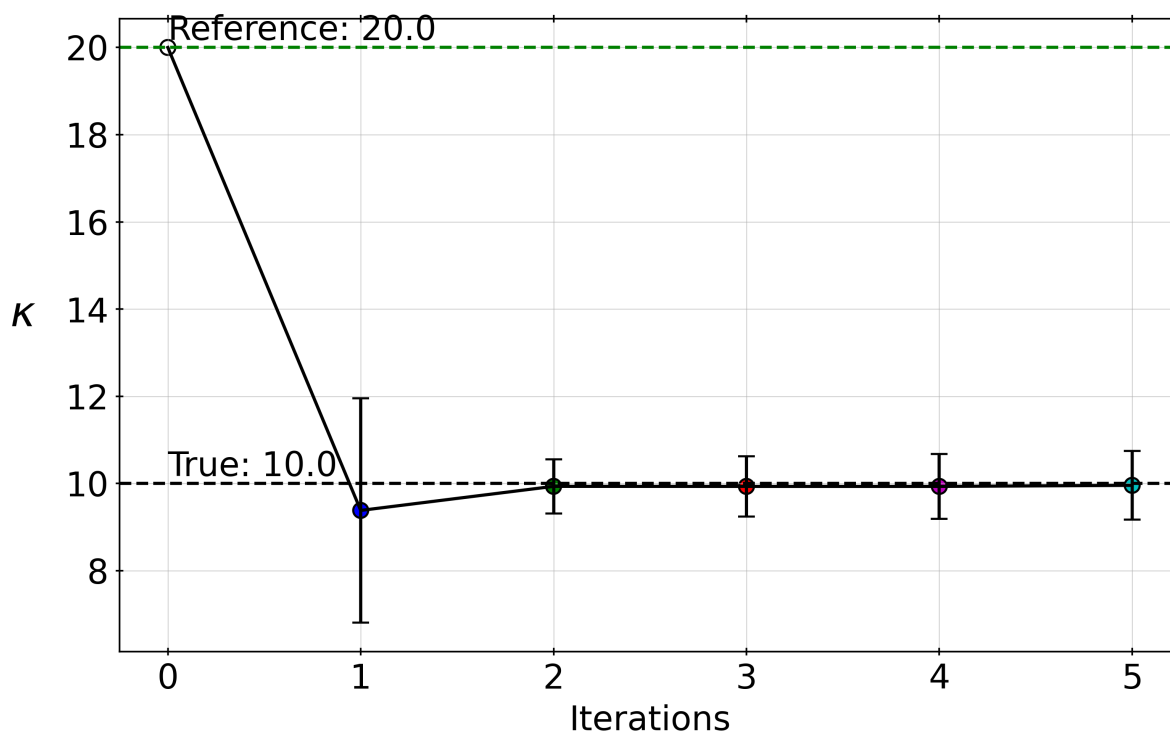


Figure S16. Refinement of the  $\kappa$ , the stiffness parameter in the KH polymer model. An initial parameter value,  $\kappa^0 = 20$ , was established. Employing second-order optimization via the ‘trust-ncg’ method, convergence to the “true” parameter,  $\kappa^* = 10$ , was achieved within a few iterations. The computations used 200 replicas and 100k MCMC steps, encompassing 500 configurations. Parameter uncertainties throughout each iteration were estimated from the inverse Hessian. These results successfully replicate the outcome of BioFF by Kofinger and Hummer.<sup>3</sup>